

Analyzing Brain Signals for Robot Control

Katrine Linnea Nergård



Thesis submitted for the degree of
Master in Informatics: Robotics and Intelligent Systems
30 credits

Institute for Informatics
Faculty of mathematics and natural sciences

UNIVERSITY OF OSLO

Spring 2021

Analyzing Brain Signals for Robot Control

Katrine Linnea Nergård

© 2021 Katrine Linnea Nergård

Analyzing Brain Signals for Robot Control

<http://www.duo.uio.no/>

Printed: Reprosentralen, University of Oslo

Abstract

Brain-computer interfaces (BCIs) enable machines to be controlled by brain signal activity. Electroencephalogram (EEG) devices are widely used to record these signals. In the last few years, several wireless EEG headsets have been commercialized, providing speed, ease of use, affordability, and mobility. The focus of this study is EEG-based motor imagery BCIs. These are systems controlled by signals that are evoked upon the imagination of movement.

It has been shown that imagining movement triggers the same areas in the brain as when generating the movement [54]. High accuracy scores have been achieved for large body parts. However, discriminating finer movements within the same limb has shown to be a more challenging task. Being able to do this would however, increase the number of available control signals significantly, paving the way for a more practical BCI.

In this thesis, EEG signals were collected from nine subjects performing executory and imagery grasping tasks with both dominant and non-dominant hands. The signals were analyzed using traditional state-of-the-art methods, and well-validated convolutional neural networks, designed for limited data.

The main classification problem was between two grasping tasks under two different conditions, the left-hand side and right-hand side. Using automatic channel selection based on a Riemannian geometry criterion prior to feature extraction and/or classification revealed a significant difference in accuracy with regards to hand-side for the majority of the subjects. There was no clear trend as to what side was more accurate, this was dependent on either the subject, algorithm or session.

An accuracy of 70% is assumed to be a required threshold for BCI applications [14]. Five out of nine subjects achieved accuracies above this threshold for classification within the same limb. This indicates that the possibility of utilizing EEG-based BCIs for single-limb classification without handcrafted features should be further investigated.

Preface

In this master thesis, brain signals are analyzed with the objective to examine the effect of hand dominance for a set of motor imagery grasping tasks. The report has been written at the Department of Informatics, Robotics and Intelligent systems during the spring semester of 2021.

The project is undertaken together with neuroscience experts at the Department of Psychology at the University of Oslo. In general, the interest lies in developing models that use brain signals to either predict mental states or provide some control functionality. The ambition is to inform the development of using thoughts in human-machine/robot interfaces.

Acknowledgement

First and foremost I want to thank my partner, Per Sondre Sodeland, and my family for the love and support through all my years as a student. Secondly, I would like to thank everyone who provided me with valuable input at the Department of Psychology when setting up my experiment.

A warm and special thanks to all the volunteers participating in the experiment. And thanks to Henrik Eijsink for introducing me to the EEG lab, and for the company during the writing of this report.

Last but not least I want to express my sincere gratitude to Professor Jim Tørresen who has provided me with guidance and resources.

Katrine Linnea Nergård, June 2021

List of Abbreviations

- BCI Brain Computer Interface.
- BMI Brain Machine Interface.
- BCIC Brain Computer Interface Competition.
- EEG Electroencephalography.
- ECoG Electrocorticography.
- MEG Magnetoencephalography.
- fMRI Functional magnetic resonance imaging.
- fNIRS Near infrared spectroscopy.
- PET Positron emission tomography
- MI Motor Imagery.
- SNR Signal to noise ratio.
- SMR Sensorimotor rhythms.
- ERD Event-related desynchronization.
- ERS Event-related synchronization.
- ERDS ERD/ERS.
- ERP Evoke Related Potential.
- EOG Electrooculography.
- EMG Electromyography.
- CSP Common Spatial Pattern.

FBCSP Filter Bank Common Spatial Pattern.

RG Riemannian Geometry.

TS Tangent Space.

LR Logistic Regression.

TSLR Tangent Space and Logistic Regression.

PCA Principal Component Analysis.

LDA Linear discriminant analysis.

SVM Support Vector Machines.

AUC Area under the curve.

ROC Receiver operating characteristic.

CNN Convolutional neural network.

RNN Recurrent neural network.

FCN Fully connected neural network.

DNN Deep neural network.

GAN Generative adversarial network.

AE Autoencoder.

DL Deep learning.

LH Left hand.

RH Right hand.

Contents

1	Introduction	1
1.1	Background and Motivation	2
1.2	Objectives	3
1.3	Contributions	4
1.4	Limitations	4
1.5	Structure of the Report	5
2	Background	7
2.1	Introduction to brain-computer interfaces	8
2.1.1	Categories of BCIs	9
2.2	The human brain	11
2.3	Electroencephalography (EEG)	12
2.3.1	Neural oscillations	13
2.4	BCI paradigms	15
2.4.1	Motor imagery	16
3	Data sets	21
3.1	Publically available data sets	22
3.2	Creating a new dataset	24
3.2.1	Subjects	24
3.2.2	Experimental protocol	25
3.2.3	Data Acquisition	26
3.2.4	Recorded EEG signals	27
3.2.5	Potential challenges	29
3.3	Preliminary data analysis	29
4	Signal Processing	33
4.1	A general EEG signal processing pipeline	34

4.1.1	Feature extraction	36
4.1.2	Feature selection	37
4.1.3	Features for oscillatory activity	37
4.1.4	Classifiers	39
4.2	Deep learning for EEG analysis	40
4.3	State-of-the-art methods	42
5	Methods	43
5.1	Processing the data	44
5.1.1	Selecting trial segment	44
5.1.2	Scaling	45
5.1.3	Data augmentation	45
5.2	Filter Bank Common Spatial Patterns (FBCSP)	46
5.3	Riemannian Geometry (RG)	48
5.4	Convolutional neural networks	48
5.4.1	EEGNet	48
5.4.2	DeepConvNet	49
5.4.3	ShallowConvNet	50
5.5	Channel selection	50
5.6	Subject handling	51
5.7	Validation procedure	51
5.8	Performance measures	51
6	Experiments and results	53
6.1	Experiments	54
6.2	Results	55
7	Discussion	62
7.1	Ethical considerations	65
7.2	Future work	67
8	Summary and conclusion	68
A	Appendix	70

List of Figures

2.1	Number of publications over the years based on a search with the keyword “brain computer interface” on PubMed [61].	8
2.2	Electrode types that have been used for BCIs: EEG from scalp, ECoG from brain surface, and cortex-penetrating microelectrodes. [47]	9
2.3	Illustration of human brain lobes.	12
2.4	BioSemi cap layout, based on the international 10-20 system, 64+2 channels. [28]	14
2.5	Brain wave samples with dominant frequencies belonging to beta, alpha, theta, and delta bands. [7]	15
2.6	The international 10–20 system of EEG electrode placement overlaid on the somatotopic organization of the sensorimotor cortex [74].	18
2.7	Sensory Homunculus and Motor Homunculus sculptures at the Museum of Natural History, London. They illustrate what a man would look like, if each part of him grew in relation to the area of the cortex that controls it.	19
2.8	Examples of modulated mu rhythm signals. A) illustrates the difference in topographical distribution on the scalp when performing actual right-hand movement. B) illustrates imagined movement corresponding to A. C) depicts rest by the dashed line and imagery movement by the solid line. D) shows the corresponding r^2 -spectrum for rest vs. imagined movement. [65]	20
3.1	Experimental setup.	25

3.2	Illustration of the four grasping tasks, and the experimental protocol of a single trial.	26
3.3	Brain waves recorded from one of the subjects in the experiment, illustrating common artifacts. a) No artifacts. b) Eye blink artifacts. c) Electrooculography (EOG) artifacts. d) Electromyography (EMG) artifacts.	28
3.4	Evoked MI data for channel C3 and C4, Subject 1, band-pass filtered to mu rhythm.	30
3.5	ERDS map, mu and beta band, LH	31
3.6	ERDS map, mu and beta band, RH	31
3.7	ERDS values for left hand and right hand classes in channels C3 and C4 (subject 1).	32
3.8	Topography of CSP pattern, and corresponding spectrum of RH movement versus rest for subject 3.	32
4.1	Illustration of a classical EEG signal processing pipeline for motor imagery-based BCI.	34
5.1	Subject 1, LH/RH classification, 2s sliding windows with 0.5 overlap. Showing variation of accuracy over the course of the trial.	45
5.2	CSP-filtered signals. Filters 1 and 2 maximize the variance of signals from left hand MI, while minimizing right hand MI. Filters 3 and 4 maximize variance of right hand MI and minimize left hand MI. [40]	47
5.3	Visualization of the EEGNet architecture. [34]	49
6.1	Accuracy of implemented algorithms for 4-class problem using BCIC 2a dataset, averaged over all folds and all subjects.	56
6.2	Accuracies for best performing subjects of the different cases, all models included. Error bars denote the standard deviation of the folds. The dotted line indicates chance level.	61
7.1	Accuracies for best performing subjects of the different cases, with each run used as unseen test data.	66

List of Tables

3.1	Publically available MI EEG datasets	23
3.2	Entire experimental procedure	27
6.1	LH-RH case: Accuracies averaged accross all subjects and all folds. Best performing experiment marked in bold for each model.	57
6.2	LH-LH case: Accuracies averaged accross all subjects and all folds. Best performing experiment marked in bold for each model.	57
6.3	RH-RH case: Accuracies averaged accross all subjects and all folds. Best performing experiment marked in bold for each model.	58
6.4	4-class case: Accuracies averaged accross all subjects and all folds. Best performing experiment marked in bold for each model.	58
6.5	LH-RH case: Accuracies of individual all subjects averaged over all folds. Accuracies above 70% are marked in bold.	58
6.6	LH-LH case, with Riemann channel selection, 8 channels: Accuracies of individual all subjects averaged over all folds. Accuracies above 70% marked in bold. The multiple scores for subjects 3 and 4 reflects the different sessions.	59
6.7	RH-RH case, with Riemann channel selection, 8 channels: Accuracies of individual all subjects averaged over all folds. Accuracies above 70% marked in bold. The multiple scores for subjects 3 and 4 reflects the different sessions.	59

6.8 4-class case;, with Riemann channel selection, 8 channels: Accuracies of individual all subjects averaged over all folds. In this case, random chance is at 25%. The multiple scores for subjects 3 and 4 reflects the different sessions. 60

7.1 RH-RH accuracies subtracted from LH-LH accuracies. . 64

1 Introduction

In this chapter an introduction to the general outline of the report is given, along with motivation and objectives for the study.

The chapter is divided into five sections. Section 1.1 provides basic background knowledge and motivations. Section 1.2 states the objectives. Section 1.3 describes the contributions of this work. Section 1.4 the limitations. Finally, section 1.5 presents the overall structure of the report.

1.1 Background and Motivation

Humans controlling machines with their minds become a reality through brain-computer interfaces (BCIs). A BCI is a system that translates brain activity into commands for an interactive application. Many application areas have the potential to be revolutionized, such as control of assistive technologies for severely motor-impaired users, rehabilitation for stroke patients, gaming devices, and adaptive human-computer interfaces reacting to the mental state of the user, to name a few.

Both startups and established companies are racing to strengthen the link between humans and machines. In 2017, Facebook announced that they would be investing in the development of non-invasive, wearable BCIs that would allow users to "type with their brains". Elon Musk, one of the founders of Neuralink, expressed in 2019 that the company wants to start by treating brain injuries and eventually "achieve a symbiosis with artificial intelligence".

Brain activity is often captured using electroencephalography (EEG), and there is a growing interest in the commercialization of EEG products for BCI applications. Several new electrode headsets designed for speed, ease of use, comfort, and mobility in real-world environments, have entered the market in the last few years.

A number of control signals can be employed in a BCI system, divided into different paradigms. Motor imagery (MI) signals are generated when imagining a motor task. Research has confirmed that imagining a movement activates the same area in the brain as when actually generating the movement [54]. This study will be limited to EEG-based BCIs following the motor imagery paradigm.

Promising results have been obtained for distinguishing between the MI tasks of large body parts. The number of commands that can be decoded corresponds to the number of MI tasks that can be distinguished by the BCI system. The ability to discriminate between finer motory tasks would largely increase the number of available commands and hence the functionality of such a BCI. One of the motivations in this thesis is to serve as a stepping stone towards increasing the number of available commands. Popular competitions,

such as Kaggle’s Grasp and Lift EEG Detection Competition from 2015, and the 2020 International BCI Competition, where participants were asked to decode single-limb related motor imagery, illustrate the field’s growing interest in this particular topic.

There are several challenges to overcome in the development of more practical BCIs. EEG signals are noisy, non-stationary, and the data is highly complex. Also, the statistical distribution of MI data is highly variable across subjects, runs, and sessions. Hence a calibration process with hand-engineered feature extraction techniques has traditionally been necessary to achieve acceptable performances by the classifier. Emerging deep learning techniques has, however, shown great promise in tackling these challenges. They do not rely on hand-engineered features and can merge feature extraction, selection, and classification. Sometimes they require no preprocessing and can be used to build subject-independent systems with no calibration time, dealing with highly complex data. The literature shows that Convolutional Neural Networks (CNNs) have been the most popular choice, but advantages compared to traditional EEG processing approaches, remain unverified [60].

1.2 Objectives

This project shall research both traditional approaches and convolutional neural networks to classify an EEG dataset collected explicitly for this study. Principal understanding of the oscillatory activity based brain-computer interfaces will be emphasized.

The main objective is to determine whether finer motory tasks are easier to classify when executed/imagined with the non-dominant hand compared to the dominant one. Another objective is to determine whether such finer motor tasks on a single limb can reach acceptable performance criteria to pass as additional commands in a BCI. There is a consensus in the field that the required accuracy level for real-world application is around 70% [14, 33, 37].

To establish a baseline, current state-of-the-art algorithms in traditional machine learning will be explored and compared to a novel, promising EEG-tailored convolutional neural networks. Different data

augmentation- and feature selection techniques will be explored.

The following research questions have been formulated:

1. Does hand-dominance affect the discriminative properties of a set of hand grasps?
2. To what extent do tasks within the same limb reach decoding accuracies above the required threshold ($\sim 70\%$) for BCI applications?

1.3 Contributions

The main contributions related to this work are:

- A dataset containing EEG signals of single-limb movements, with the potential to contribute in other experiments than those limited to this project.
- Increased knowledge on the effect of hand dominance when decoding upper-limb motor imagery tasks. A thorough search of relevant literature yielded no existing articles on this matter.
- A comparison of different models and various approaches for performance enhancement.

It is more challenging to classify MI tasks related to a single limb than tasks of different limbs. This is due to the high similarity of the recorded signals and the proximity of the cortical regions emitting those signals. Very few publicly available datasets include finer motory tasks within the same limb, making the collected dataset and the following classification experiments a contribution to the field.

1.4 Limitations

The work presented in this report can be considered an early-stage feasibility study, to provide insight as to whether further research is worthwhile. The results are limited by the small amount of available data, focusing only on a few tasks.

1.5 Structure of the Report

Chapter 1: Introduction

The introduction presents the general outline of this report, as well as motivation and objectives for the study.

Chapter 2: Background

A basic introduction to brain-computer interfaces (BCI), the human brain, and electroencephalography (EEG) is given in this chapter, along with relevant application areas. Finally, different paradigms are described, focusing on motor imagery.

Chapter 3: Data sets

This chapter provides an overview of key distinctions of publicly available datasets belonging to the motor imagery paradigm and a thorough description of the EEG experiment conducted to collect data. Finally, some preliminary analysis results are presented.

Chapter 4: Signal Processing

A description of a general EEG-based processing pipeline, followed by the current state-of-the-art in traditional machine learning and an introduction to relevant deep learning techniques for classification.

Chapter 4: Methods

An overview of the pre-processing steps performed in this study, together with details on the implemented models.

Chapter 6: Experiments and results

This chapter presents details about all the conducted experiments and their results. A comparison of the implemented models is made.

Chapter 7: Discussion

An evaluation of the results and ethical dilemmas. Research questions are answered. Recommendations for further research are also given.

Chapter 8: Summary and Conclusion

This chapter presents the conclusion of this study by summarizing the results.

2 Background

This chapter introduces some of the core aspects of brain-computer interfaces, including relevant knowledge of brain anatomy and methodology for recording and deploying brain signals.

The chapter is split into four parts. First, section 2.1 gives a general introduction to brain-computer interfaces. Section 2.2 dives into the human brain and its anatomy. Section 2.3 introduces electroencephalography, the most widely used recording technology for brain activity. Finally, section 2.4 presents different approaches for utilizing various control signals from the brain, called paradigms. The focus is mainly on motor imagery.

2.1 Introduction to brain-computer interfaces

Brain-Computer Interfaces (BCIs) are systems that translate a measure of human brain activity into a command or message for an interactive application to a connected machine.

Hans Berger recorded the first human electroencephalogram (EEG) in 1924 [42]. This opened completely new possibilities for the research of human brain activities. The term "BCI" was introduced in 1973 by Jacques Vidal [76]. Since then, many researchers have attempted to interpret brain waveforms to establish more convenient and accurate control over external devices. Due to advances in new technology, the interest in the field continues to grow. Over the years, this has resulted in many concepts, methods, paradigms, and applications. There has also been a significant increase in the number of publications in the last decade, see Figure 2.1.

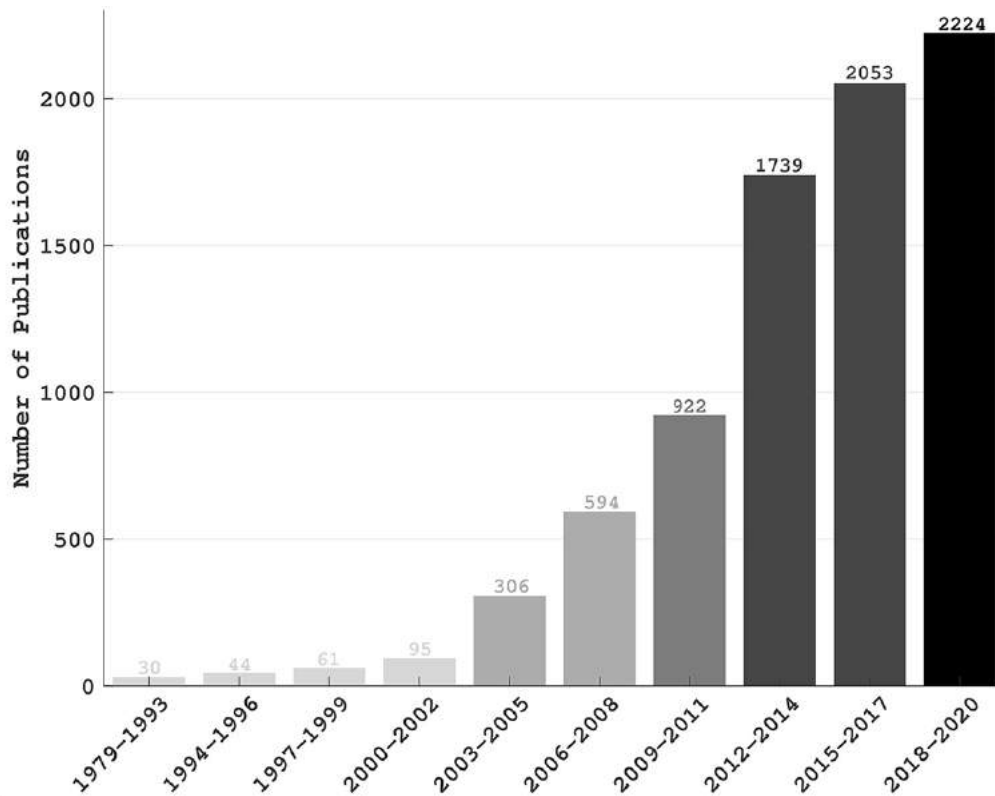


Figure 2.1: Number of publications over the years based on a search with the keyword “brain computer interface” on PubMed [61].

BCIs can be divided into various types and categories. A dependent

BCI uses brain signals that depend on existing output pathways, such as muscle activity [78]. An independent BCI does not depend on such pathways, i.e., the message is not carried by peripheral muscles and nerves. Actual muscle activity is not needed. The brain signals alone are sufficient. Independent BCIs are of great theoretical interest, as they provide the brain with new output pathways. For people with severe neuromuscular disabilities, sometimes lacking all normal output channels, independent BCIs can be very useful.

2.1.1 Categories of BCIs

There are several different techniques for measuring brain signals. They can be divided into invasive, semi-invasive, and non-invasive.

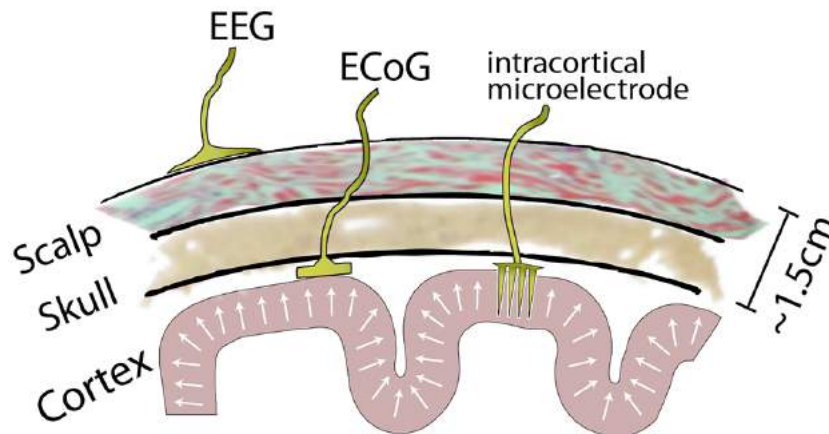


Figure 2.2: Electrode types that have been used for BCIs: EEG from scalp, ECoG from brain surface, and cortex-penetrating micro-electrodes. [47]

Invasive

Neurosurgery is an invasive method, where microelectrodes are implanted under the skull and into the brain. Such a microelectrode is illustrated in Figure 2.2. Small grids of electrodes are directly implanted in, e.g., the motor cortex or related areas. Then, a motor imagery strategy can be used to induce brain activity changes and subsequently control movements of a robotic arm [70]. Single-unit BCIs detect signals from a single area of brain cells, and multi-unit BCIs detect from multiple areas.

Most research in this field has been performed on animals, mainly monkeys and rats, but some systems have also been demonstrated in humans. Recordings acquired from invasive techniques benefit from having a very high signal-to-noise ratio and spatial resolution, resulting in significantly improved system performance. Many challenges do, however, arise. As a reaction to the foreign object, the body can build a scar around the electrodes, and this can cause signal deterioration. Both high cost and high risk follow neurosurgery, making the target of such BCIs mainly patients with particular needs. [51]

Semi-invasive

A technique that requires a craniotomy to implant the electrodes is defined as semi-invasive. Electrodes are placed on the exposed brain surface, and electrical activity from the cerebral cortex is recorded using electrocorticography (ECoG). See Figure 2.2. A grid or strip of electrodes covers a large area of the cortex, and the method is used in a range of cognitive studies. ECoG studies in BCI are mostly limited to cases where the primary need for surgery comes from other reasons, e.g., epilepsy.

In a study from 2006 [12], electrodes were implanted in the frontal regions of epileptic patients. The patients were asked to perform imagery tasks for mouth, tongue, and hand. Using ECoG, the BCI system was able to classify the imagery tasks after one single session.

This activity recording involves lower clinical risk than the invasive one, as the electrode array does not penetrate the cortex. The signals show robustness over long recording periods [77], high spatial resolution and signal fidelity and resistance to noise. Muscle and eye movement do not affect the recording, as it does with EEG.

Non-invasive

There are multiple non-invasive techniques used to record brain signals, where EEG is the most common. With EEG technology, the signals are recorded without any penetration as the sensors are placed on top of the scalp, see Figure 2.2. The electric activity of the brain is measured with high temporal- and low spatial resolution. EEG is a popular choice for building BCIs due to its deployability, low cost, and

ease of integration with other technologies [18, 46]. See section 2.3 for more details.

Examples of other non-invasive techniques include magnetoencephalography (MEG), positron emission tomography (PET), functional magnetic resonance imaging (fMRI), and near-infrared spectroscopy (fNIRS). MEG measures the brain's magnetic activity, and fMRI, PET, and NIRS rely on changes in blood flow. PET and MEG have a high spatial and temporal resolution. fMRI and NIRS have a high spatial resolution but poor temporal.

These techniques can be used in a BCI system, but they are expensive and technically demanding, and not commonly used. The focus of this study will be on EEG-based brain-computer interfaces.

2.2 The human brain

The human brain works as a set of sub-systems cooperating to control the various functionalities of the whole body. Information about the external environment is received through our senses, such as hearing, sight, taste, smell, and touch. Certain parts of the brain are associated with distinct cognitive functions.

The brain can be generally divided into two main parts - the cerebral cortex and the subcortical regions [56]. Subcortical regions are those areas that control the basic and vital functions such as heart rate, body temperature, respiration, and emotional responses, including fear, reflexes, learning, and memory. The cerebral cortex is considered newer in terms of evolution. It is the largest and the most complicated part of the brain. This part is the focus of most BCI research since the control of sensory and motor processing happens here and higher-level functions such as language processing, pattern recognition, planning, and reasoning.

The cerebral cortex is the outer layer of neural tissue of the cerebrum of the brain [81]. It is the largest site of neural integration in the central nervous system and contains 14 to 16 billion neurons. The longitudinal fissure divides the cerebrum into the left and right cerebral hemispheres. Each hemisphere can be divided into four main lobes, as illustrated in Figure 2.3, namely the frontal, parietal,

temporal, and occipital. They correspond to different brain functions.

Functions of the frontal lobe are organizing, planning, social skills, flexible thinking, conscious movement, problem-solving, emotional and behavioral control, and attention [56]. The parietal lobe handles functions such as spatial awareness, perception, spelling, and objects classification. The basic functions of the temporal lobe understand language, facial recognition, memory, hearing, vision, speech, and emotions. Finally, the occipital lobe interprets visual stimuli.

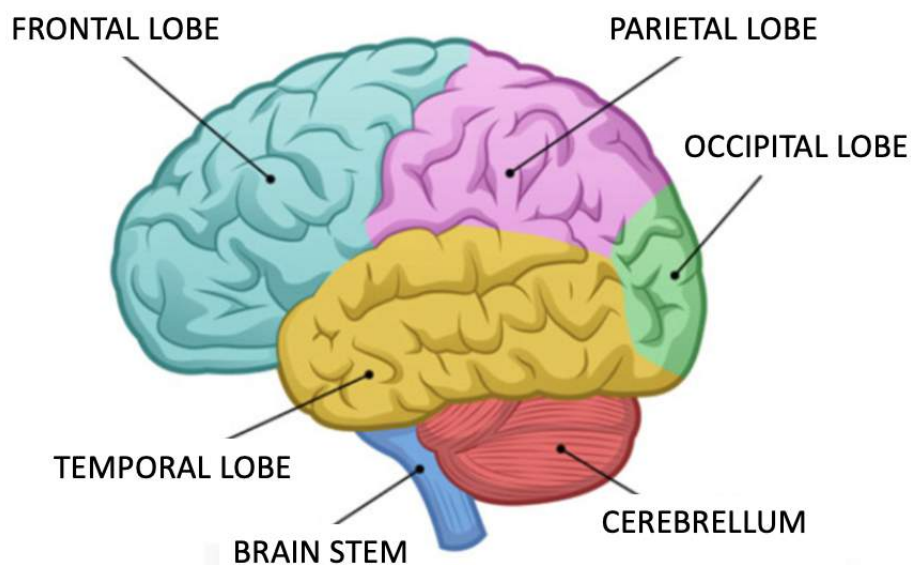


Figure 2.3: Illustration of human brain lobes.

The brain is constantly generating electric signals. The skull and skin of the head are excellent electrical insulators, making it difficult to record from individual neurons. However, when a large number of neurons do the same thing simultaneously, it is possible to see the activity with electrodes placed on the scalp's surface [63].

2.3 Electroencephalography (EEG)

In an EEG recording, electrodes are placed on the scalp's surface to pick up the electrical current generated by the brain. As mentioned in section 2.2, when groups of neurons fire together, they provide enough signal to be measured from on top of the scalp. Hence, only clusters of neurons can be measured.

The electrodes are small metal plates made from various materials, such as tin, silver, gold, or platinum. Specifically, what is recorded is the voltage difference between a minimum of two electrodes. The electrodes acquire the signal from the scalp, amplifiers process the analog signal to enlarge the amplitude of the EEG signals so that an A/D converter can digitalize the signal more accurately. Finally, the recording device displays/stores the data.

The spatial resolution reflects the ability to localize the precise brain regions generating a signal. In EEG, it is determined by the number of electrodes used. When a higher spatial resolution is required, typically, at least 32 electrodes are used, all the way up to 500. In general, spatial resolution for EEG is low (compared to, e.g., ECoG and fMRI) because the signal needs to travel through different layers up to the skull, and the activity registered by an electrode is a mixture of different signals generated by various brain regions. The resolution, however, can be improved using certain types of filters or by combining EEG with other tools (e.g., fMRI). High spatial resolution is not necessarily needed, and commercial headsets often use fewer electrodes.

EEG does, however, have excellent time resolution. It is possible to take thousand of snapshots of electrical activity across different sensors in a single second.

Electrodes can be placed following the international 10–20 system (see figure 2.4) to ensure data is always collected from the same region. This is recommended as a standard layout. 10–20 refers to specific anatomic landmarks or inter-electrode distance, such that it is 10–20% of the front-to-back or right-to-left head perimeters. Other systems, such as 10-10 and 10-5, could be valid standards as well [30].

2.3.1 Neural oscillations

EEG data contains rhythmic activity, which reflects neural oscillations. These oscillations are divided into frequency bands. Today there are mainly five established bands. These are gamma (γ), beta (β), alpha (α), theta (θ) and delta (δ), see figure 2.5. Research has found associations between these rhythms and different brain states [1].

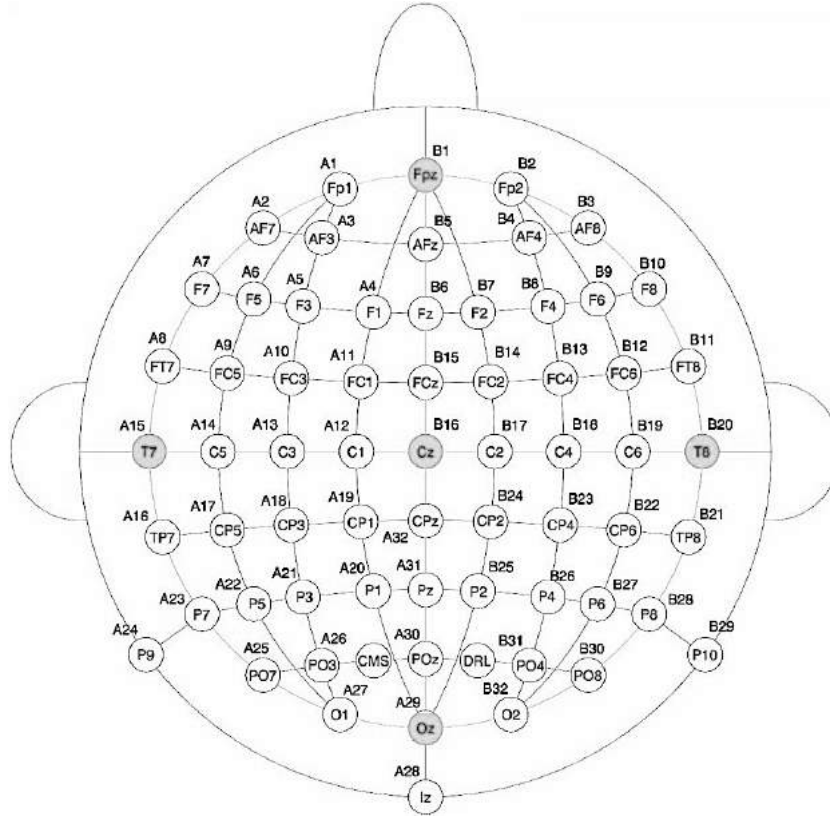


Figure 2.4: BioSemi cap layout, based on the international 10-20 system, 64+2 channels. [28]

- **Gamma** can be detected at the somatosensory cortex with a frequency greater than 30 Hz. It is present during problem-solving and other cases where concentration is required.
- **Beta** is associated with being alert, busy, and having an active mind. It falls in the range between 12-30 Hz.
- **Alpha** has frequencies between 8-12 Hz. It is usually associated with relaxation, reflectivity. When the alpha activity is recorded over the sensorimotor region, it is in the literature known as mu (μ) activity. Suppression of this signal indicates that motor neurons are working.
- **Theta** frequencies fall within the range of 4–7 Hz. It is associated with drowsiness and deep meditation.
- **Delta** has a frequency range of 1–4 Hz. It is associated with deep sleep and dreaming.

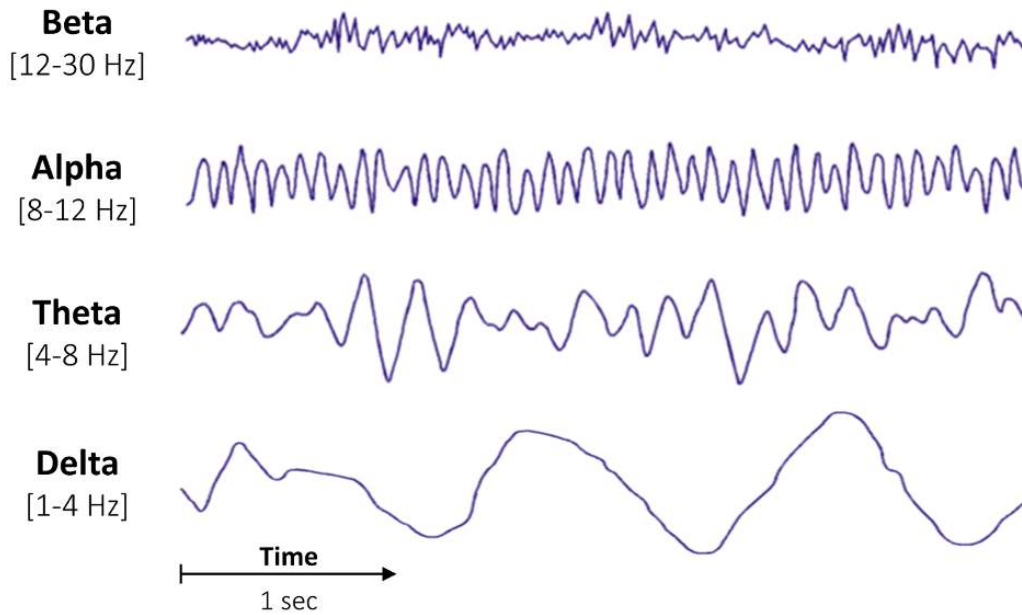


Figure 2.5: Brain wave samples with dominant frequencies belonging to beta, alpha, theta, and delta bands. [7]

2.4 BCI paradigms

BCIs are implemented using different approaches, often referred to as paradigms. The desired application needs to be matched with the appropriate control signal. The paradigm of choice should be convenient, reliable, and accurate.

EEG-based BCIs can be either evoked or spontaneous [31, 50]. Evoked systems depend on external stimulation, such as sensory, auditory, or visual stimulation. To determine the user's will, the BCI system's response evoked by the stimuli is identified. In spontaneous BCIs, on the other hand, no external stimulation is required. The control actions are based on the decoding of activity produced as a result of mental activity. Most users can master evoked systems, they typically require fewer sensors and training, and have higher throughput than spontaneous systems. However, the required gaze on fixed stimuli and concentrations that follows can be tiring [49].

The two main categories of evoked EEG systems include event-related potentials (ERPs) and visually evoked potentials (VEPs). ERPs are brain signals responses to sensory or cognitive events, VEPs are brain signals responses to a visual stimulus [49, 72]. One of the most

widely researched areas of VEP-based BCIs is steady-state visually evoked potentials (SSVEPs). To induce SSVEP, users can be exposed to frequency flickering stimulus and have to shift their attention and gaze on the desired target. This paradigm requires no training, and the stimuli may flash in many different frequencies, leaving room for a large number of discrete commands. A study on the usability of an SSVEP-based system [69] performed a survey of 32 subjects, where 48% thought the system was easy to use, 52% found stimuli annoying, and 66% considered the system to require a lot of concentration in use.

An ERP is derived by averaging EEG signals induced by a specific event. P300 is the most studied ERP and one of the most popular paradigms in BCI systems based on EEG [49]. The P300 wave is a positive deflection in the ERP. Usually, it is elicited in an “oddball” paradigm when a subject is presented with a regular train of standard stimuli and detects the occasional target stimulus. However, the system’s maximum throughput is restricted by the dependence of several stimuli, which adds to the computational time taken for decision-making [50].

Motor Imagery (MI) BCI is the most common example of a spontaneous BCI. The paradigm requires the user to imagine limb movement. Research has confirmed that imagining a movement activates the same area in the brain as when actually generating the movement [54]. A drawback is the training process involved for the subjects to learn how to modulate specific frequency bands of neural activity.

The experiments in this thesis follow the motor imagery paradigm. Hence it will be focused on in greater depth.

2.4.1 Motor imagery

MI is mostly based on sensorimotor rhythms (SMR) [2]. The subject imagines movements of certain body parts, such as tongue, hands, and feet. The motor imagery task being carried can be identified from mu and beta activity changes within the recorded EEG signals [25]. This can be utilized in, e.g., prosthetic device control. Different areas of the cortex control different parts of the body. How much of

the cortex relates to each part of the body can be illustrated through a cortical homunculus, see Figure 2.6. This is basically a distorted representation of the human body, based on neurological mapping of the proportions and areas of the human brain dedicated to processing motor- or sensory functions for different body parts. The distorted size of certain features correlates to how richly innervated that region is.

For better visualization of the proportions, see the 3D version of the homunculus in Figure 2.7. The size of the hands in the motor homunculus implies that especially different hand movements should theoretically be distinguishable, since such a large part of the brain is dedicated to this particular task. This is part of the reason why hand gestures were chosen as the objective for this study.

When the motor cortex or somatic sensory cortex are not producing motor output or processing sensory information, they typically exhibit rhythmic activity at a frequency between 8-12 Hz, as seen in human EEG measurement. As specified in 2.3.1, this is normally called the alpha band, but when recorded from the sensory-motor cortex, it is called the mu rhythm. BCIs utilizing internal electrodes can reliably use gamma activity for MI classification. When using scalp EEG, the recorded gamma signals do not reach the scalp with sufficient integrity to be utilized.

When activity in a particular band decreases, this is called event-related desynchronization (ERD), while an increase in a particular band is called event-related synchronization (ERS) [52]. ERD and ERS can be triggered by motor/sensory output or input [53]. There is typically a decrease in the mu activity over the sensorimotor cortex contralateral upon preparation for movement or actual movement. The same changes can be seen when imagining movements, i.e., they can occur independently of the brain's output to peripheral muscles and nerves, making them highly relevant for BCI applications.

Figure 2.8 illustrates the difference in topographical distribution on the scalp when performing actual right-hand movement, 2.8A, and corresponding imagined movement, 2.8B. In 2.8C, rest is depicted by the dashed line and imagery movement by the solid line. 2.8D shows the corresponding r^2 spectrum for rest vs. imagined movement. Signal modulation is focused on the frequency bands associated with the mu

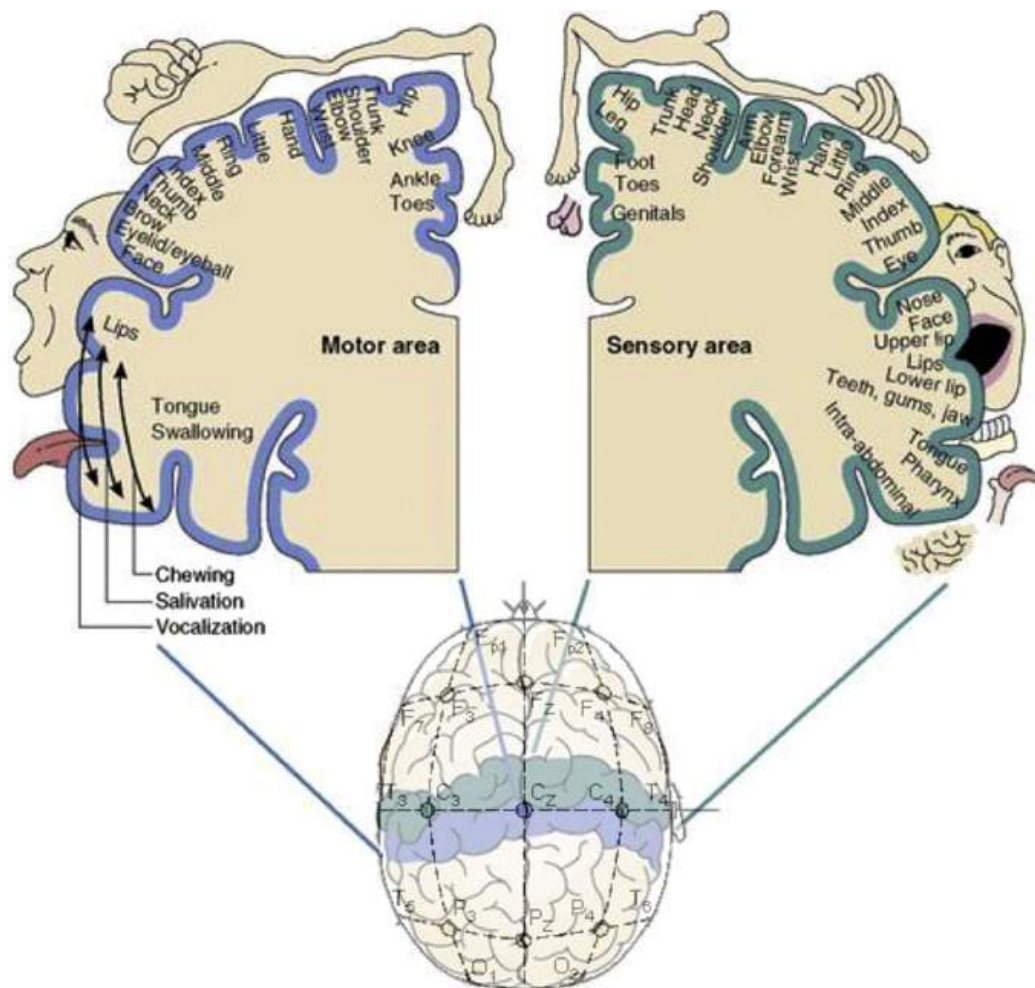


Figure 2.6: The international 10–20 system of EEG electrode placement overlaid on the somatotopic organization of the sensorimotor cortex [74].

rhythm and over the sensorimotor cortex.

The hand area of the motor cortex is the origin of the mu rhythm. In addition, there is a similar rhythm originated from the foot area, located between the hemispheres. Hence the mu rhythm of a human can be influenced by hand or foot movement imagination [65]. The signals of hand movements are most prominent in electrode locations C3 and C4 in the 10/20 international system and Cz for foot movement, see Figure 2.4. These electrodes are located above the sensorimotor cortex, see Figure 2.6.

The initial goal of MI-based BCI research was to create new means of communication for paralyzed people. Such patients can use, e.g.,

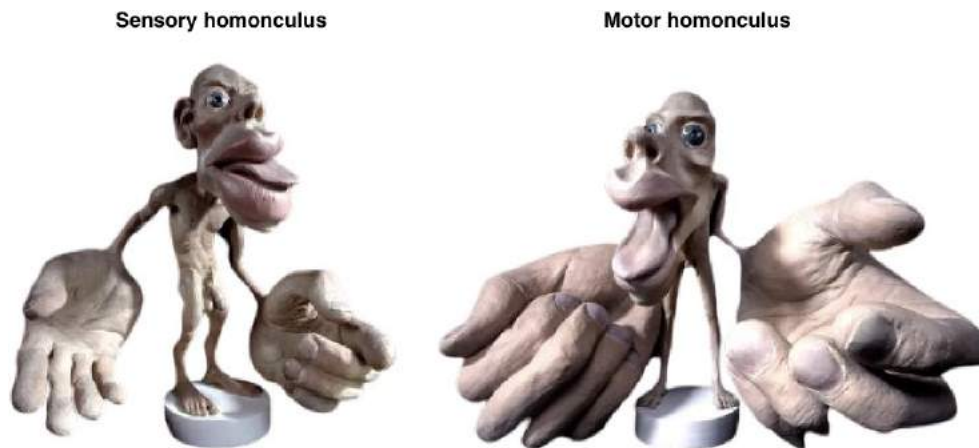


Figure 2.7: Sensory Homunculus and Motor Homunculus sculptures at the Museum of Natural History, London. They illustrate what a man would look like, if each part of him grew in relation to the area of the cortex that controls it.

left- and right-hand MI to answer yes and no. Today many researchers study MI for neurorehabilitation after stroke. MI neurofeedback has proven effective in reestablishing motor movements. MI BCIs also have the potential to compensate for persistent sensory and motor deficiencies. There are several examples in the literature where SMR has been employed. To name a few: cursor control [45], opening and closing a prosthetic hand with imagining right or left hand-movement [27], foot imagery to restore one type of hand grasp [55] and controlling an artificial upper limb [3]. There are also several non-medical applications for SMR, such as gaming and controlling quadcopters or robotic manipulators.

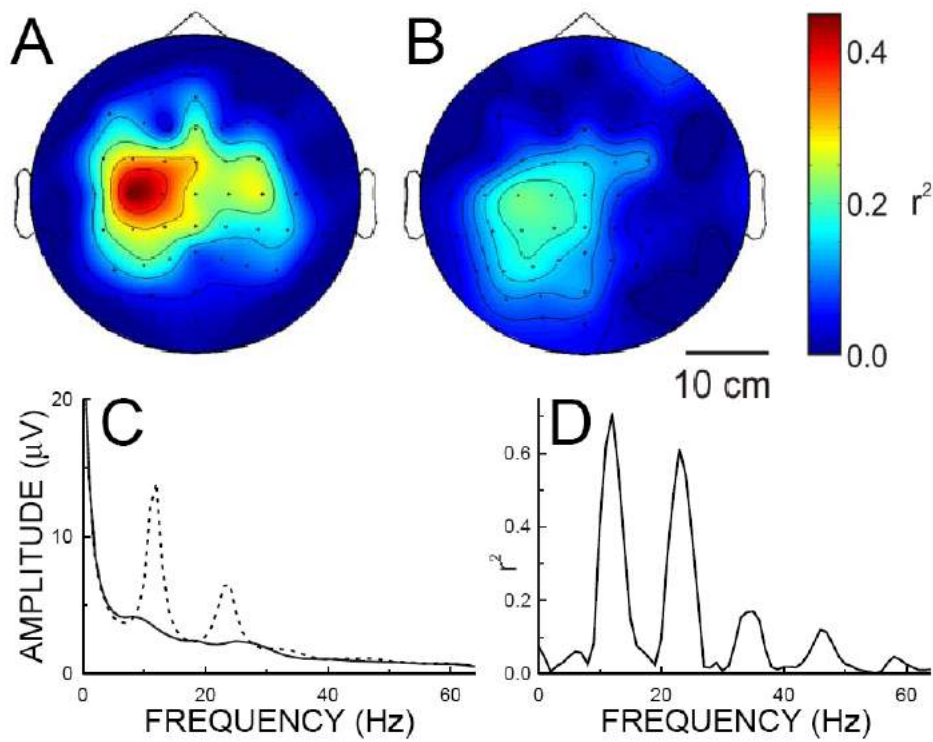


Figure 2.8: Examples of modulated mu rhythm signals. A) illustrates the difference in topographical distribution on the scalp when performing actual right-hand movement. B) illustrates imagined movement corresponding to A. C) depicts rest by the dashed line and imagery movement by the solid line. D) shows the corresponding r^2 -spectrum for rest vs. imagined movement. [65]

3 Data sets

This chapter provides an overview of key distinctions of publicly available datasets belonging to the motor imagery paradigm and a description of the EEG experiment that was set up to collect relevant data. Some preliminary analysis results are also presented.

The chapter is split into three parts. First, section 3.1 gives an overview of existing available datasets containig motor imagery tasks. Section 3.2 provides a thorough description of the data collection. Finally, section 3.3 presents some results from a preliminary analysis of the collected data, serving as a sanity check.

3.1 Publically available data sets

Available EEG datasets intended for BCIs were reviewed, both to learn the common approach in EEG data collection, and to identify potential research gaps. Several websites provide such overviews. In table 3.1, the motor imagery datasets found from `bnci-horizon-2020.eu`, `moabb.neurotechx.com`, and `openbci.com` have been listed, along with key distinctions. The main objective of BNCI Horizon 2020 is to provide a roadmap for the BCI field, serving as a guideline for future activities that will be supported by the EU research framework program Horizon 2020. Moabb is short for mother of all BCI benchmarks, aiming at building a comprehensive benchmark of popular BCI algorithms applied on an extensive list of freely available EEG datasets. Finally, OpenBCI is an open-source brain-computer interface platform.

Both the literature [59, 68] and the available datasets reveal that the vast majority of the existing MI EEG-based BCI systems have focused on differentiating between left hand, right hand, feet, and tongue. These tasks have been shown to produce significant and discriminative changes in the EEG signals relative to background EEG [25]. While the classification of them has been widely documented and validated - achieving high accuracy, the task of discriminating the motor imagery of different movements within the same limb has proven challenging [48, 79]. This is due to the fact that these motor tasks activate regions that have very proximate representations on the motor cortex area of the brain, all on the same hemisphere, see Figure 2.6. To date, not many studies have addressed this problem. A few that has [20, 22, 38, 79], does however show promising results, demonstrating the possibility of utilizing EEG signals to decode single-limb MI tasks. Nonetheless, in these studies, the motor imagery task has been conducted on one side only. The effect of hand dominance has not been considered, which is the main focus of this thesis.

Some related work includes [80], where they evaluate the effect of handedness on one simple left-hand/right-hand motor imagery task. The results indicated that lateralization of SMR during a motor imagery task differs according to handedness. Left-handers

Table 3.1: Publically available MI EEG datasets

Dataset	Tasks	No of subjects	No of sessions	No of trials per session	No of electrodes
BCIC IV 2a, 2008 [16]	Left hand Right hand Feet Tongue	9	2	6 runs \times 12 trials \times 4 tasks = 288	22
BCIC IV 2b 2008 [36]	Left hand Right hand	9	5	144 (avg)	3
BCIC III 4a, 2004 [19]	Right hand Right foot	5	1	280	118
BCIC II 3, 2002 [44]	Left hand Right foot	1	1	280	3
PhysioNet, 2009 [23]	Eyes closed Both feet Both fists Left fist Right fist	109	1	270	64
High-Gamma, 2017 [66]	Left hand Right hand Both feet Rest	14	13	1000 (total)	128
Müller-Putz et al, 2010	Right hand Both feet	13	1	8 runs \times 10 trials \times 2 tasks = 160	15
Faller et al, 2015	Right hand Both feet	12	2	5 runs \times 20 trials \times 2 tasks = 200	13
Cho et al, 2017	Left hand Right hand	52	1	5 runs \times 20 trials \times 2 tasks = 200	64
Barachant, 2012	Right hand Both feet	8	1	1 run \times 20 trials \times 2 tasks = 40	16

presented lower accuracy during BCI performance (single session) and weaker SMR suppression in the alpha band (8–13 Hz) during mental simulation of left-hand movements. In another study [43], the main objective was to identify specific hand movements from electroencephalographic activity. The effect of hand dominance was discussed, and they found statistically significant differences in classification between the dominant and non-dominant hands for some of the tasks. The research was however limited to motor execution, and additional recording devices such as an optical sensor, and a sensor glove were included.

3.2 Creating a new dataset

To address the research questions of this study, custom data had to be collected. The main motivation for better classifications of same-limb tasks is the increase in control dimensions of MI EEG-based BCI systems it would provide. A step towards a more practical BCI would be the ability to restore finer hand movements, such as different grasps from MI. A neuro-prosthesis, for instance, could be used to generate the movement once it has been decoded.

Grasp types are divided into two main categories, precision, and power. In a power grasp, all fingers and palms are activated, whereas, in a precision grasp, only the tip of the thumb and opposing finger(s) are used.

To ensure that the collected MI data is informative and high-quality, the experimental setup followed the principal guidelines provided by [17].

3.2.1 Subjects

9 right-handed, non-impaired subjects, aged between 25 and 60, participated in the EEG experiment. 5 female and 4 male. None of them had any previous experience with BCIs.

3.2.2 Experimental protocol

Before the experiment began, the subjects were instructed to imagine the kinesthetic, and not the visual experience, during the motor imagery period. As reported in [71], kinesthetic MI modulates more corticomotor excitability than visual MI does.

The cue-based protocol consisted of four different motor imagery/executory tasks, namely the imagination/execution of a left-hand cylindrical grasp (class 1), left-hand pinch grasp (class 2), right-hand cylindrical grasp (class 3), and right-hand pinch grasp (class 4). Two sessions on different days were recorded for two of the subjects.

Each session comprised of 6 runs. One run consisted of 40 trials (10 for each of the four possible classes) in a pseudorandom order, yielding a total of 240 trials per session. Two of the runs were motor execution (ME), and four of them were motor imagery (MI).



Figure 3.1: Experimental setup.

The subjects were seated comfortably in an armchair in front of a computer screen, see Figure 3.1. Each trial lasted eight seconds. At the beginning of a trial ($t = 0$ s), a fixation cross appeared on a screen. After three seconds, a visual cue in the form of an image (corresponding to one of the four classes) appeared and stayed on the screen for two

seconds, followed by a blank screen for three consecutive seconds.

This prompted the subjects to perform the desired motor imagery/execution task. The subjects were asked to carry out the motor imagery task until the fixation cross reappeared from the screen at $t = 8$ s. The protocol is illustrated in Figure 3.2.

After each run, the participants were asked to rest while seated, in order to avoid fatigue, see 3.2. No feedback was provided.

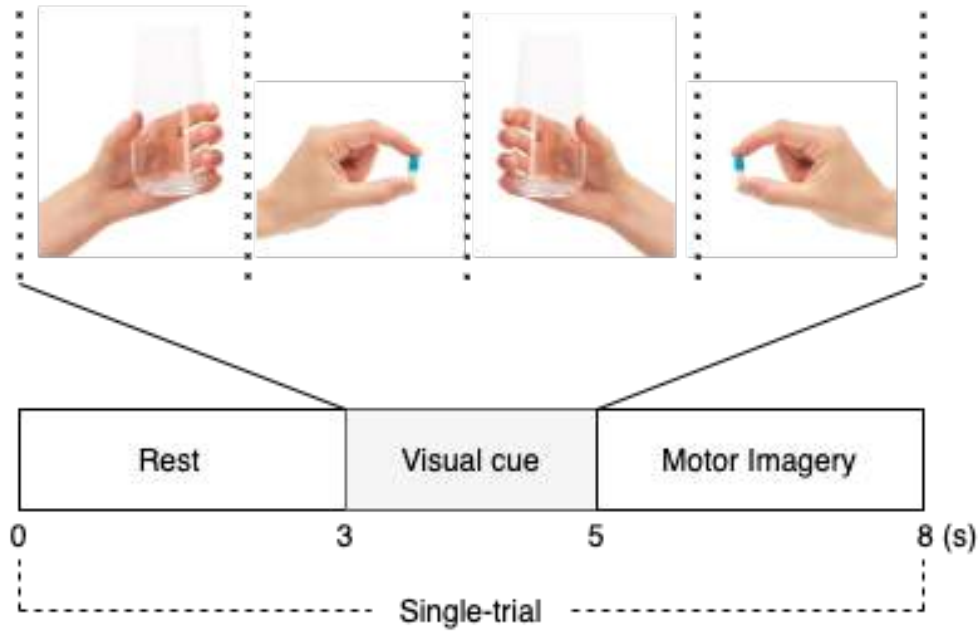


Figure 3.2: Illustration of the four grasping tasks, and the experimental protocol of a single trial.

3.2.3 Data Acquisition

The EEG data was recorded with the BioSemi ActiveTwo system, sampled at 1024 Hz.

The code for presenting instructions, and collecting trigger points was written in Matlab, using the Psychophysics Toolbox extensions [15]. A 64 channel montage was used, based on the international 10-20 system, see Figure 2.4. There is often a direct correspondence between major brain features and the positions of the electrodes in this system. When performing a sanity check of a given brain signal topology, this ability can be exploited.

Table 3.2: Entire experimental procedure

#	Task	Duration (min)
1	Filling out consent form	5
2	EEG electrode placement	40
3	Run 1 (Motor Execution)	5-6
4	Pause	3-6
5	Run 2 (Motor Imagination)	5-6
6	Pause	3-6
7	Run 3 (Motor Imagination)	5-6
8	Pause	3-6
9	Run 4 (Motor Imagination)	5-6
10	Pause	3-6
11	Run 5 (Motor Imagination)	5-6
12	Pause	3-6
13	Run 6 (Motor Execution)	5-6
14	Removing electrodes and cleaning laboratory	20
Total		105-126

3.2.4 Recorded EEG signals

Noise

High impedance can indicate poor conductivity between scalp and electrodes. The impedance of all electrodes between the skin and the sensors was maintained below 20 k Ω during the experiment.

Surrounding electronics can also induce noise to the raw brain signal, inferring the quality. Hence the amplifier runs on batteries and an optical cable leads to a computer standing outside from the shielded space where the subjects were performing the tasks.

Common artifacts

Electrical power lines use sinusoidal voltages, generally with a frequency of 50Hz in Europe. Such artifacts can be suppressed by a notch filter in the pre-processing stage.

Fast movement of the eyelid generates eye blink artifacts. These are recorded as positive peaks lasting a small proportion of a second, see figure 3.3b. They are mainly visible in the frontopolar region, but propagates, becoming weaker. So weak that these artifacts in the alpha band are negligible, producing no apparent effect on a sensorimotor

analysis. Averaged P300 waveforms, on the other hand, can be strongly influenced by them.

Movement of the eye produces electrooculography (EOG) artifacts. The effect of these artifacts are quite similar to that of eye blinking on the time- or frequency domain analysis, except that the amplitude tends to be larger, and the frequency lower, see figure 3.3c.

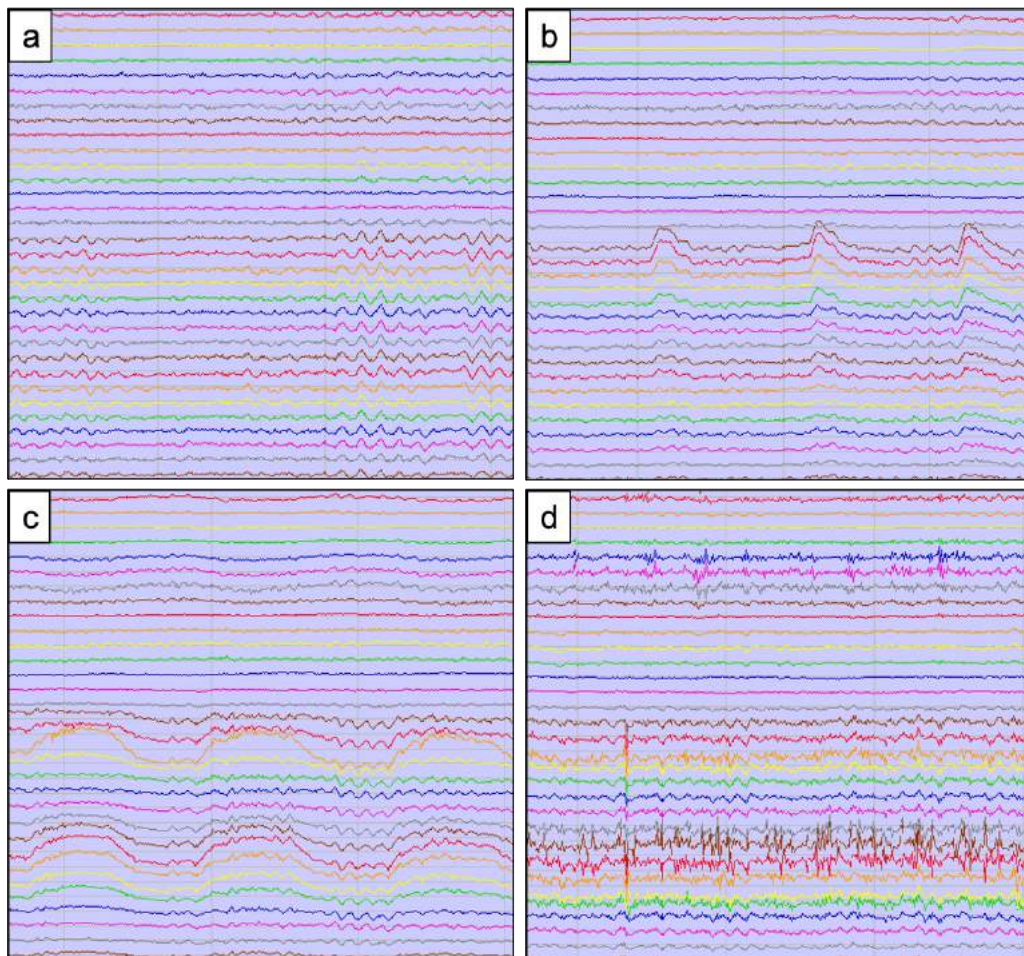


Figure 3.3: Brain waves recorded from one of the subjects in the experiment, illustrating common artifacts. a) No artifacts. b) Eye blink artifacts. c) Electrooculography (EOG) artifacts. d) Electromyography (EMG) artifacts.

Finally, muscular artifacts (electromyography, EMG) are typically caused by lifting eyebrows and closing the jaw. The effect of such artifacts can completely obscure any frequency analysis, see Figure 3.3d. To avoid jaw-generated artifacts, the subjects were asked to keep their mouths slightly open.

3.2.5 Potential challenges

BCI researchers have been interested in performance variation from subject to subject, and to provide subject-independent algorithms. A fraction (10-30% [29]) of users are BCI-illiterate, meaning that mu rhythms from their somatosensory cortex are difficult to detect. Session-to-session variability is also a challenge, so minimizing the environmental and psychological differences between training and testing can be beneficial.

3.3 Preliminary data analysis

The raw EEG-data was saved in the BioSemi .bdf format, before being preprocessed and analyzed using MNE [26]. MNE is a community-driven software package to be used as a general-purpose toolbox for processing electrophysiology data, offering tools for preprocessing, time-frequency analysis, statistics, machine learning, and data visualization.

As an initial inspection, or sanity check, of the collected data, some visualization plots were generated. EEG data can be divided into 3 main types in MNE: raw data, epoched data, and evoked (averaged) data. Continuous data is stored as a raw object containing a 2D array with dimensions of channels \times time. When the raw data is epoched, it consists of time-locked trials. These are stored in a 3D array of events \times channels \times times. Finally, evoked objects typically store EEG data that has been averaged over multiple epochs, which is a common technique for estimating stimulus-evoked activity. The data in an evoked object is stored in a 2D array of shape channels \times times. Thus to create an evoked object, the raw data of runs 2-5 (motor imagery) for all the subjects was epoched, then all the epochs from one condition were averaged together.

It is expected to see a contralateral decrease in the mu/beta rhythm activity in channels C3 and C4 upon imagination/execution of left-hand or right-hand movement. Figure 3.4 shows evoked left hand and right-hand data, over channels C3 and C4 for subject 1. The activity decrease caused by right-hand motion (orange) in C3, is particularly pronounced

around 0.5s, 2s, and 3s. Similarly, the decrease in activity caused by left-hand motion (blue) in C4, is pronounced around 2s and 4s.

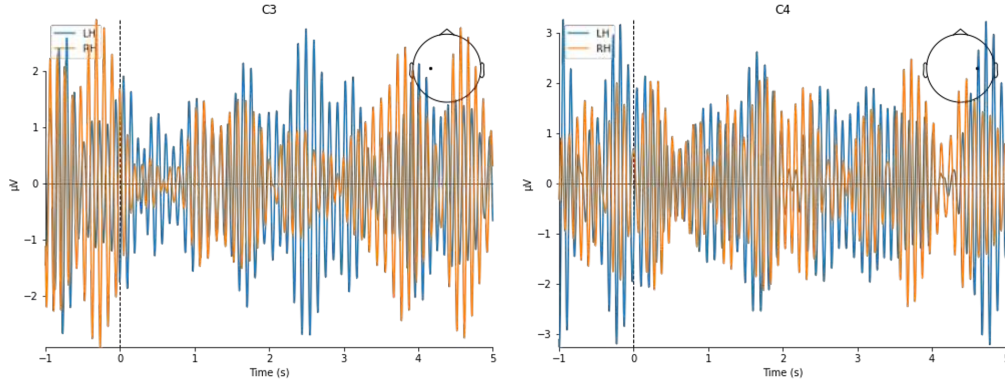


Figure 3.4: Evoked MI data for channel C3 and C4, Subject 1, band-pass filtered to mu rhythm.

ERDS (ERD/ERS) maps of event-related EEG data were also calculated and visualized. ERDS is short for event-related desynchronization (ERD) and event-related synchronization (ERS). As mentioned in chapter 2, ERD corresponds to a decrease in power in a specific frequency band relative to a baseline. Similarly, ERS corresponds to an increase in power. An ERDS map is a time/frequency representation of ERD/ERS over a range of frequencies [24]. ERDS maps were generated for left-hand and right-hand movement, considering only channels C3 and C4.

First, the data was divided into epochs of 7s in length, one second before the visual cue to one second after the end of the trial. The maps were computed for frequencies ranging from 7 to 26Hz, to cover the most relevant frequency bands. ERD was mapped to red color, and ERS to blue color, which is the convention in many ERDS publications. Finally, cluster-based permutation tests were performed to estimate significant ERDS values.

The ERDS maps reveal contralateral suppression in both the mu and beta band for both left- and right hand movement. In 3.5 the contrast between the channels is more significant than in 3.6. It should also be noted that the beta band (14-30) provides more distinguishable characteristics than the alpha band in this case.

Confidence bands are plotted in 3.7, for mu and beta frequency

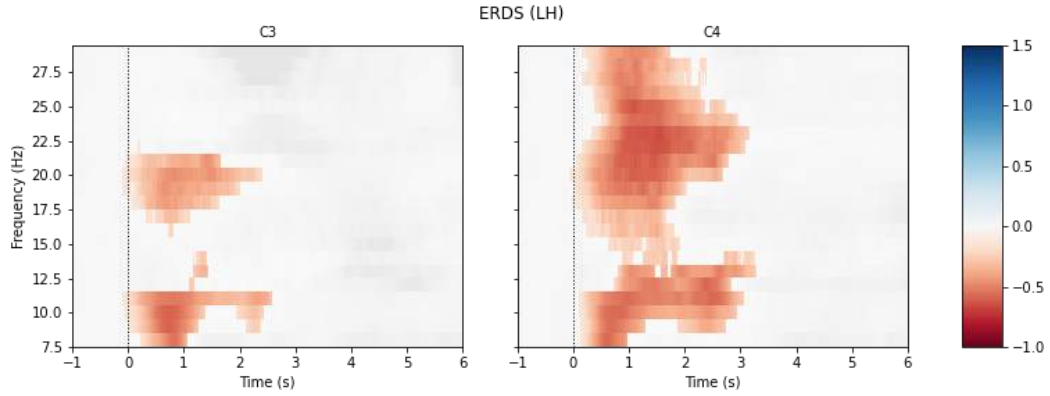


Figure 3.5: ERDS map, mu and beta band, LH

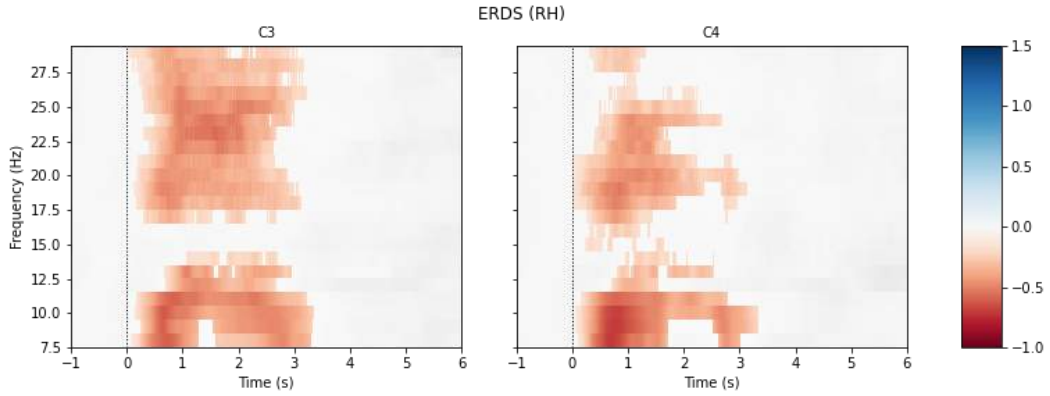


Figure 3.6: ERDS map, mu and beta band, RH

bands. ERDS is lower for right-hand class (orange) in channel C3, and the other way around for channel C4, as is to be expected from the literature. Similar to what could be seen from the ERDS maps, the distinction between the two classes is more evident in the beta band than in the mu band for this particular subject.

Using Common Spatial Patterns (CSP) algorithm (for more details, see chapter 5), spatial filters can be extracted that maximize the difference of variance before and during the movement, and then visualize the corresponding spectrum. The resulting CSP topography and spectrum for subject 3 can be seen in 3.8. The CSP pattern corresponding to the left motor cortex (right hand MI) to the left, and the suppression during versus before movement to the right.

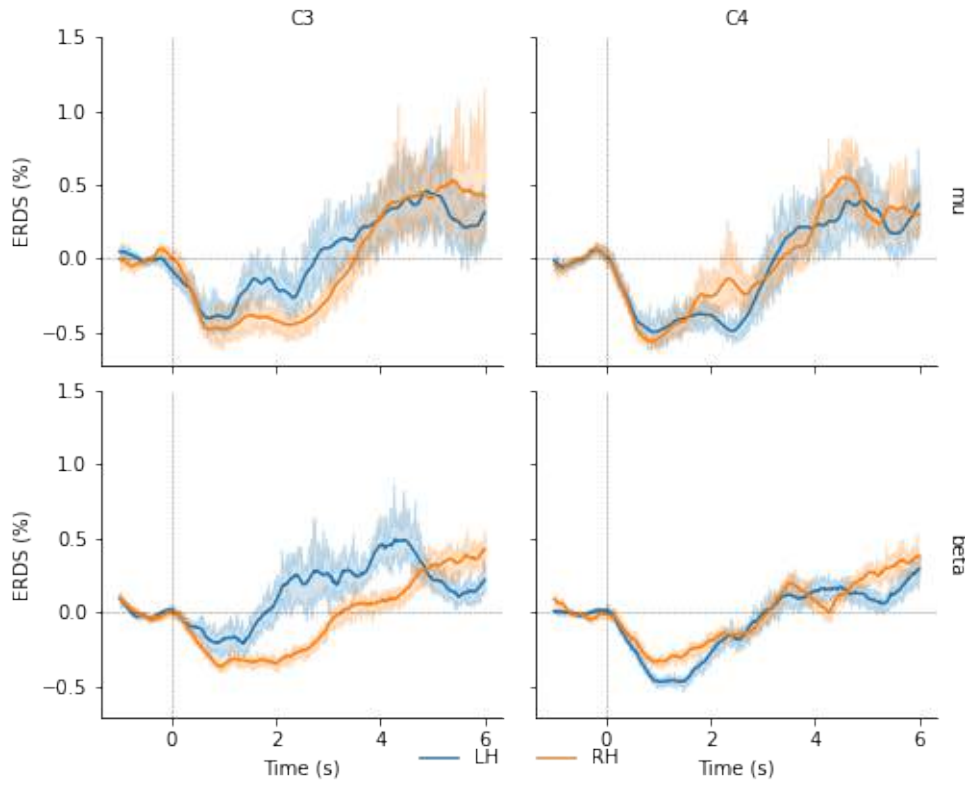


Figure 3.7: ERDS values for left hand and right hand classes in channels C3 and C4 (subject 1).

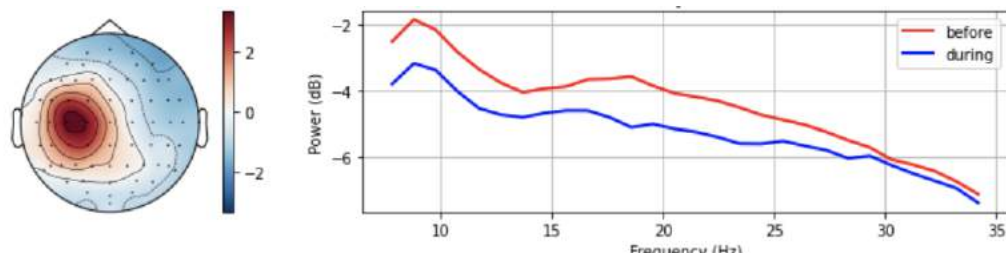


Figure 3.8: Topography of CSP pattern, and corresponding spectrum of RH movement versus rest for subject 3.

4 Signal Processing

A conventional processing pipeline for brain-signal decoding as a supervised classification problem is first presented. This is followed by a general introduction to deep learning, with special attention to convolutional neural networks. Finally, current state-of-the-art methods are established.

The chapter is split into three parts. First, section 4.1 gives a description of a general EEG-based processing pipeline. Section 4.2 presents an introduction to relevant deep learning techniques for classification of EEG signals. Finally, section 4.3 sums up the current state-of-the-art methods.

4.1 A general EEG signal processing pipeline

Figure 4.1 illustrates the signal processing carried out in a traditional MI EEG-based system. Raw EEG data is usually pre-processed to some degree to remove noise and/or artifacts, but this is not always the case. Then features are extracted, and in some systems, the most salient feature is selected before classification. Finally, the classifier attempts to classify the motor imagery task performed by the user. Feature extraction and selection techniques will be discussed in greater detail in the following sections.

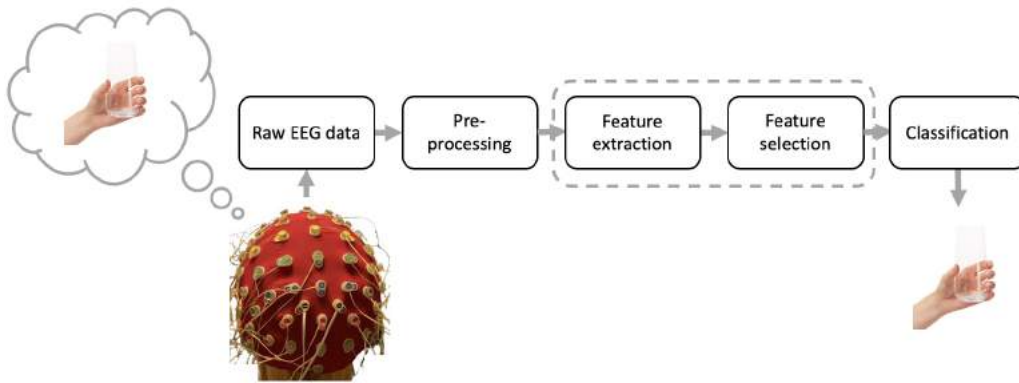


Figure 4.1: Illustration of a classical EEG signal processing pipeline for motor imagery-based BCI.

There are four mental states to identify in the motor imagery experiment of this thesis - left-hand power grasp, right-hand power grasp, left-hand precision grasp, and right-hand precision grasp.

These states, are typically identified using band power features. These represent the power of the signal in a specific frequency band. As mentioned in section 2.4.1, these features are usually extracted from the μ -band, at around 8 to 12 Hz, and the β -band, at around 16 to 24 Hz, when the tasks are motor imagery. Selected electrodes are generally C3 and C4, for right and left-hand movements, respectively. Finally, these features can be classified using e.g. logistic regression.

Two phases are generally required in order to make use of a BCI - an offline training and calibration phase, and an online operational phase, with a translation of brain activity patterns into computer commands. In an online BCI system, a user produces some specific EEG pattern,

e.g. through motor imagery, and these signals are recorded. Then they are typically pre-processed using various spectral, temporal, and spatial filters. In order to represent the signals in a compact form, different features can be extracted. Finally, they are classified and translated into a command for some applications. The user gets feedback on whether the mental command was recognized or not.

Today, in order to obtain a reliable BCI system, offline calibration is often used. Usually, optimal features are selected, and the classification algorithm is tuned on pre-recorded training data. Most BCIs are tuned specifically for each user, as EEG signals are highly user-specific. The training data typically consists of an EEG signal that has been recorded while the user performs mental tasks of interest several times, based on the instruction. Offline calibration will be used in this thesis.

The curse of dimensionality means that with a fixed number of training samples, the average expected predictive power of a classifier first increases as the number of features/dimensions used increases, but beyond a certain dimensionality it starts deteriorating instead of improving steadily. There is an exponential increase in the amount of data needed for a proper description of the different classes with the dimensionality of the feature vectors.

When using machine learning on a finite number of data samples in high-dimensional feature space (each feature having a range of possible values), typically a large amount of training data is required to ensure that there are multiple samples with each combination of values. A rule of thumb is that, for each dimension in the representation, there should be at least 5 training examples [75].

In the setup of this thesis' experiment, with 64 electrodes, a sampling rate of e.g. 128 Hz (after downsampling), and one trial being 1 second long, the dimensionality of the feature space would be $64 \times 128 = 8192$, which again would require at least 40960 training samples. This amount of data is not available, hence it is necessary to represent EEG signals in a compact manner when using traditional machine learning algorithms. Relevant features can be extracted before being fed to a classifier. Typically the signals are filtered in both spatial- and time domains, before extracting the features.

4.1.1 Feature extraction

Timepoint features and frequency band power features are commonly used to represent EEG signals. Timepoint features are EEG samples from all channels that are concatenated. They are typically extracted after band-pass filtering and downsampling. Timepoint features are a common choice to classify ERPs, for use in P300-based BCIs.

Band power features represent a signals' power for a given channel and frequency band, averaged over a time window. Such features are extensively used in BCI systems where oscillatory activity, such as changes in rhythm amplitude, is being exploited. Band power features are considered the gold standard for MI-based BCIs, and several other passive BCIs made for decoding mental states, or SSVEP-based BCIs [39].

Both of these features should be extracted after some sort of spatial filtering. Spatial filters combine the original sensor signals, usually linearly. Well-known spatial filters include principal component analysis (PCA), independent component analysis (ICA), and common spatial patterns (CSP) [13, 32, 57]. The latter is dedicated to band-power features and BCIs intended for oscillatory activity and is used in this work.

In traditional EEG-based BCIs, spatial filtering followed by either time point or band power feature extraction, is by far the most common choice, though many other methods have been explored. Combining various types of features can lead to higher classification accuracy, but also increased dimensionality. This means that only the most relevant features should be selected, in order to mitigate the curse of dimensionality.[11].

To summarize, there are three main sources of information where features can be extracted from EEG signals:

- *Spatial information:* Features describing spatially where the signals are coming from. Then focus can be on signals originating from a specific area of the brain. Practically, this would mean selecting certain channels of interest.
- *Spectral/frequential information:* Features describing the variance of the power in some relevant frequency bands.

- *Temporal information:* Features describing how the relevant signal varies with time. In practice, this means using signal values from different time windows or points.

For motor imagery, spectral and spatial features are the most commonly used sources of information.

4.1.2 Feature selection

There are several benefits from selecting a subset of the previously extracted features. To name a few:

- Some features may not be related to the targeted mental states, or redundant.
- There is a positive correlation between the number of parameters that the classifier has to optimize and the number of features. The risk of overtraining can be reduced.
- It is easier to detect which features that are related to the targeted mental state.
- Computational efficiency and reduced data storage.

For example, frequency band selection has provided improvements for MI-based BCIs, using maximal mutual information. Some frequently used feature selection approaches include support vector machine (SVM) for channel selection, genetic algorithms for spectral feature selections, linear regressor for knowledge extraction, and evolutionary algorithms for feature selection.

4.1.3 Features for oscillatory activity

A basic MI BCI system access spatial information by extracting features only from electrodes located over the motor areas of the brain. Typically these channels are C4 for left-hand movements, C3 for right-hand movements, and Cz for movement of the feet. The spectral information can be exploited through a focus on specific frequency bands. These are generally the mu band, between 8 and 12 Hz, and the beta band, between 16 and 24 Hz.

More precisely, for a BCI that can recognize left-hand MI versus right-hand MI, the basic features extracted would be the average band

power in 8 to 12 Hz and 16 to 24 Hz from both channels C3 and C4. Hence, a BCI may be able to recognize left and right MI using EEG signals only described by four features.

A basic design, such as the one described above, is however not optimal. When only using two channels, relevant information measured by other channels gets lost. Also, C3 and C4 may not be the best channels for the specific subject. The same logic applies to the fixed mu- and beta bands, they may not be the optimal frequency bands for the subject at hand. Subject-specific designs, where the choice of channels and frequency bands are optimized for this subject, generally perform better. It is also known that performance is improved when using more than two channels, as this enables the collection of relevant information spread across various EEG sensors.

In [64], it is suggested that optimal performances are achieved by using a larger number of channels, for example, 48. Interestingly, with as little as 8 channels, reasonable performances in motor imagery had been obtained [6, 64]. However, no fundamental rules have been established as to what is the required number of electrodes for a specific application, so the number used in various studies is usually arbitrary [60]. Adding more electrodes would increase the spatial resolution, but to what degree is of interest as the preparation time, patient inconvenience and device cost also increase.

A blurred image of the signals that originated from within the brain is represented through the EEG signals measured on the scalps' surface. Due to the smearing effect of the brain and skull, the underlying signal is spread over multiple EEG channels. Spatial filtering may help in recovering the original signal that is spread over various channels through a linear combination of them.

Blindly adding more channels will however not solve the problem. The increase of dimensionality that follows channel addition may actually decrease the performance, because of the following increase in dimensionality. In order to exploit several EEG channels efficiently, three main approaches are available. All of them contribute to reduced dimensionality [40]:

- *Feature selection algorithm:* Automatic subset selection of rele-

vant features, among the previously extracted features.

- *Channel selection algorithms:* Automatic subset selection of relevant channels, among the available channels.
- *Spatial Filtering algorithms:* Generally, a small number of new channels are defined as a linear combination of the original ones.

4.1.4 Classifiers

Linear discriminant analysis (LDA) and support vector machines (SVM) have been the traditional choices for BCI classification algorithms, particularly for real-time and online BCIs.

The main challenges for EEG-based classification methods are the low signal-to-noise ratio and variation over time, users, and runs. There is also generally a limited amount of training data available for calibration of the classifiers, and still an overall low performance and reliability of BCIs. For addressing these challenges, several methods have been studied. For instance, adaptive classifiers, where the parameters are updated incrementally while new EEG data becomes available. This method deals with the non-stationarity of the EEG signal and requires less offline training data.

Another method is transfer learning, where the aim is to transfer features or classifiers from one domain to another, e.g. from one subject to another, or from one session to another. In this way, the challenges of the low amount of training data and variability between and within subjects, are addressed.

Finally, new methods are explored to compensate for poor reliability and low signal-to-noise ratio. These include matrix and tensor classifiers, as well as deep learning. These methods explore the possibility of merging feature extraction, selection, and classification, by processing the signals and classifying them in one step. In addition, a couple of miscellaneous methods should be mentioned, namely random forest and shrinkage LDA (sLDA). The latter has shown to be superior to LDA across a number of BCI datasets. These classifiers have shown to be especially effective with little training data. [39]

4.2 Deep learning for EEG analysis

Deep learning (DL) techniques have shown a great capacity for learning useful feature representations from raw data. In an EEG context, this can be a propitious aid in making sense of the recorded signals. DL algorithms can merge feature extraction, selection, and classification and hence not rely on subject-dependent, hand-engineered features. They have the potential to provide subject-independent classification, that requires little to no pre-processing and calibration, with the ability to overcome data with high complexity.

Deep learning models use successive layers to progressively extract higher-level features from raw input. A deep neural network (DNN) contains multiple layers between input and output layers. Types of neural networks can vary, but the components are the same: synapses, neurons, functions, biases, and weights. Well-known network types include fully connected- (FCN), convolutional- (CNN), and recurrent neural network (RNN). Layers of artificial neurons are stacked, each applying a linear transformation to the data they receive, followed by a non-linear activation function. The parameters are learned through the minimization of a loss function. The input in EEG data is usually formatted as an n -dimensional array with dimensions $n = c \times l$, where c is the number of EEG-channel and l is the number of samples (typically in μV). In a classification problem, the output represents the number of classes. A potential workflow could be to perform preprocessing and feature extraction of the input array before it is fed into the neural network.

In fully connected networks, the activations from every single neuron in a layer are fed as input to each neuron in the proceeding layer. In convolutional layers, the neurons in a given layer only see a subset of activations from the preceding one. This structure works very well for data with a spatial structure. Recurrent neural networks, in their most basic form, make use of the temporal structure by providing the layers with current activations from the preceding layer, as well as their own activations from a previous timestep.

For unsupervised tasks, where no labels are available, other architectures can be used. Some examples are generative adversarial

networks (GANs) and autoencoders (AEs). In GANs, a generator attempts to create fake examples from an unknown distribution of interest, then a discriminator tries to discriminate between real and fake data. An equilibrium is reached when the discriminator no longer can distinguish between real and fake data, because the probability distribution approximated by the generator converges to the real data distribution. Autoencoders try to reproduce their input, given some constraint, such as sparsity or artificial noise. In that way they learn a representation of the input data.

In most studies, CNNs have been the architecture of choice. Such networks have had great success in other fields, such as computer vision. Another reason for their popularity could be their capability of simultaneously training both a feature extractor and a classifier, i.e. end-to-end supervised feature learning. It is the preferred architecture when using raw EEG data as input. GANs are also typically used with this sort of data. When using frequency-domain features as input, deep belief networks are a common choice. Independent of the input, there is an increase in the interest of RNNs for EEG analysis. Also in combination with CNNs.

According to [60] it is most common to utilize up to 10 layers in a deep learning architecture for EEG analysis. Compared to the common depth of networks used in areas such as computer vision, the tendency in EEG deep learning is that shallower models achieve better performance. There are however many dependencies, such as task, amount of data, network architecture, hyperparameters, and computational resources.

Deep learning has the potential to both extend and improve processing methods that exist today. The higher-level features that can be extracted from DNNs could be more expressive or effective than what can be engineered by humans. The possibility of applying such models directly on raw data would also boost the application repertoire. In several domains, DL has surpassed the previous state-of-art, e.g. image analysis. One of the main enablers of deep learning research is however the availability of large datasets. It is assumed that a considerable amount of data is required for EEG signals, due to their high dimensionality. Given the high cost of EEG data collection, it is

crucial to understand what the equivalent amount of required data for high performance in deep learning is compared to performance in other domains.

The computational complexity and training time of deep neural networks (DNNs) are also challenging for use in practical online BCI applications. Thus, fast training is required, or, perhaps a more valuable alternative, designing universal DNNs that do not require any user-specific training. Another challenge is that the drawbacks that accompany EEG, such as low SNR, are not present in other kinds of data where DL has excelled. Hence current architectures and approaches might not be readily applicable to EEG analyses.

4.3 State-of-the-art methods

Current state-of-the-art methods include filter bank CSP (FBCSP) and Riemannian geometry. When evaluating the performance of novel deep learning networks, these are the algorithms to compare to. Deep learning methods are currently lagging in performance for BCI, given the limited training data that is available. Shallow networks do however show promise, and deep learning approaches are also relevant for data augmentation through generative adversarial networks (GANs), and end-to-end domain adaptation. Riemannian geometry classifiers (RGCs) and FCSPs considered the golden standard for several BCI problems, including motor imagery. [39]

5 Methods

In this chapter preprocessing and various augmentation techniques used in the experiments are presented. Along with a thorough description of the implemented algorithms.

The chapter is split into eight parts. First, section 5.1 describes the pre-processing of the data. Section 5.2 explains basic concepts of filter bank common spatial patterns. Section 5.3 briefly explains the basic principals of Riemannian geometry. Section 5.4 introduce the convolutional networks EEGNet, DeepConvNet and ShallowConvNet. Section 5.5 describes the procedures used for channel selection. Section 5.6 discuss subject handling. Section 5.7 discuss the validation procedure that is used. Finally, section 5.8 discuss performance measures.

5.1 Processing the data

To provide a realistic picture of performance, minimal pre-processing was applied on all subjects, there was no tailoring for specific subjects. First, potential power line noise at 50 Hz (Europe) was removed with notch filtering. Then the data was high-pass filtering with a cutoff frequency of 2 Hz to remove baseline drift.

Before feature extraction or classification, the raw data was epoched into 3D arrays consisting of time-locked trials. The epochs were then bandpass filtered to select the desired band(s), before being downsampled to 128, in accordance with the MNE software's best practice [26]. To avoid the reduction in temporal precision of events that comes with resampling a raw data object, and also avoid the edge artifacts that come with filtering an epoch object, the best practice is to first low-pass filter the raw data at or below the desired sample rate, then decimate the data after epoching, by passing the 'decim' parameter to the epochs constructor. 0.2 seconds in the beginning and end of each trial were cropped away to remove possible acute artifacts.

Testing was performed with re-referencing using both Cz as reference channel, and the average of signals from all electrodes (called common average). None of these increased the performance, so no re-referencing was used in the presented experiments.

Bad epochs were automatically rejected by defining a threshold of 800e-6V for peak-to-peak amplitude and flat signal detection.

5.1.1 Selecting trial segment

A window that is widely used in the literature is [0.5,2.5] s post cue [34, 41, 58, 62]. Before any channel or feature selection is applied, each trial is shaped with a size of (64, 256), i.e. 64 channels, and 256 samples in a 2s window with a sampling frequency of 128. The findings in section 3.3 further supports this choice of segment, see Figures 3.5, 3.6 and 3.7. The ERDS maps show that the motor imagery induced activity repression is clearly most prominent in this time segment. By using epochs that start 0.5s after cue onset one also avoids classification of responses evoked by the visual cue.

Further, a set of classifiers were tested on a sliding 2s-window with 0.5 second overlap, showing best performances when starting around 0.5 to 1.5 seconds. See Figure 5.1 for the results of subject 1 in this study.

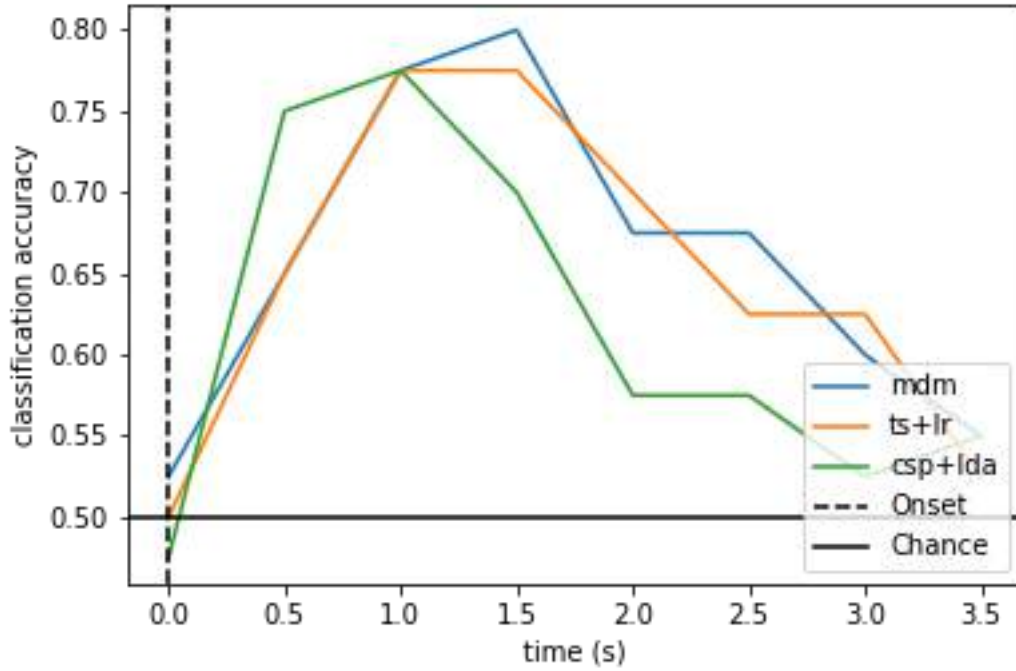


Figure 5.1: Subject 1, LH/RH classification, 2s sliding windows with 0.5 overlap. Showing variation of accuracy over the course of the trial.

5.1.2 Scaling

The data was scaled and normalized to zero mean and unit variance using z-score. This can speed up convergence. The built-in function `Scaler` in MNE [26] was used, which scales each channel using mean and standard deviation computed across all of its time points and epochs. Due to scaling sensitivity in deep learning, the data was multiplied with $1e6$, converting from μV to V .

5.1.3 Data augmentation

To reduce overfitting and to allow the use of more complex deep learning models, new data examples can be artificially generated. This

is called data augmentation, and can lead to better generalization abilities and increased stability and accuracy.

Some examples of augmentation methods seen in the literature include generated artificial EEG signals using a conditional generative adversarial network (cDCGAN) on one of the motor imagery datasets from the BCI competition [82]. This augmentation improved the accuracy from around 83% to 86% when using a CNN for classification. Several other studies have augmented their data through overlapping windows. One study compared various shift lengths, showing that generating samples through smaller shifts improved performance significantly [60]. In [21], they made use of the part of the downsampling data that is usually thrown away in the preprocessing state. With this approach, the data can be augmented by n times when downsampling by a factor of n .

Sliding window augmentations was experimented with, using two different overlaps; 0.1 and 0.5 seconds. With a 0.1s overlap, one trial was expanded to five highly correlated trials formed by the moving windows of [0.3-2.3], [0.4, 2.4], [0.5-2.5], [0.6, 2.6] and [0.7-2.7]. With 0.5s overlap, the following segments were used: [0.5-2.5], [1.0, 2.0], [1.5-3.5], [2.0, 4.0] and [2.5-4.5]. The latter segments are less correlated, and utilize the whole trial. The size of the data set is increased by five times.

Reuse of downsampled data was also tested. With an original sampling frequency of 1024 Hz, the data could be augmented 8 times, as the data was downsampled by a factor of 8, i.e. 128 Hz.

Preliminary testing was conducted based on the recommended approaches in chapter 4, to decide which classifiers to use, and what sort of feature extraction for the traditional approach.

5.2 Filter Bank Common Spatial Patterns (FBCSP)

The CSP algorithm is considered a standard tool in the repertoire of oscillatory activity-based BCIs. An increase in performance has been greatly influenced by this filter. So much that all the winning entries for all EEG datasets in the BCI competition IV (2008) used this algorithm [73].

The CSP algorithm, simply put, finds spatial filters where the variance of the filtered signal is maximal for one class, and minimal for the other. Maximizing this difference between the classes leads to optimized discriminant band-power features. The band-power of a signal in a given band is actually the same as the variance of this signal, band-pass filtered in said band. The most useful features in oscillatory activity-based BCIs are indeed band power features, making CSP particularly useful. In motor imagery, the EEG signals are typically filtered in the 8-30 Hz band (including both mu and beta), before being filtered spatially with CSP. See Figure 5.2 for illustration, the signals are CSP filtered and show a clear difference in variance, i.e. band power, ensuring increased classification performance.

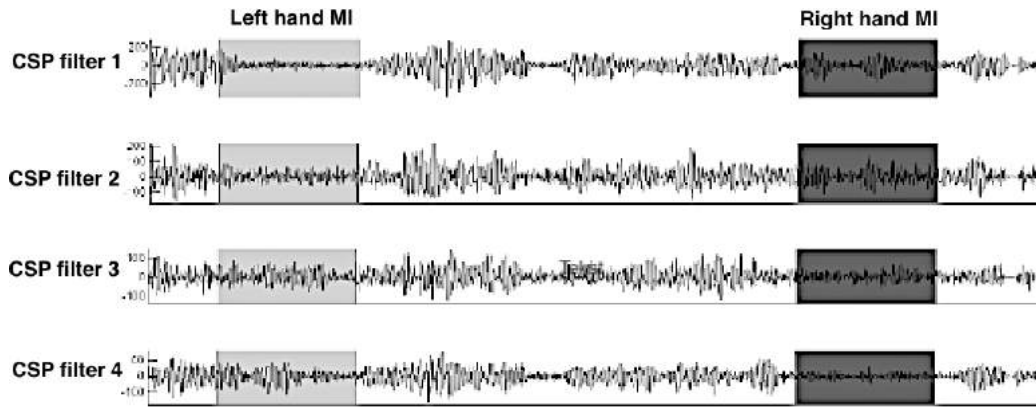


Figure 5.2: CSP-filtered signals. Filters 1 and 2 maximize the variance of signals from left hand MI, while minimizing right hand MI. Filters 3 and 4 maximize variance of right hand MI and minimize left hand MI. [40]

CSP does however also have some limitations, as it is not robust to noise and non-stationarity, and is prone to overfitting when the amount of training data is small. To make CSP more stable and robust, a variant called Filter Bank CSP (FBCSP) was introduced [4, 5]. In this method, the EEG signals are first filtered in multiple frequency bands, using a filter bank. Then the CSP algorithm is used on each of the frequency bands in the bank to optimize the spatial filters. Here both spatial and spectral information is exploited, using band power features from relevant frequency bands.

Implementation

The implementation of the FBCSP algorithm follows the description provided in [34]. First, the EEG signal was bandpass filtered into 9 non-overlapping filter banks with a step size of 4 Hz, starting at 4Hz. Hence the following banks were created: 4-8Hz, 8-12Hz, 12-16Hz, 16-20Hz, 20-24Hz, 24-28Hz, 28-32Hz, 32-36Hz, and 36-40Hz.

Second, 4 CSP filters was trained with a one-versus-rest strategy, using Ledoit wolf regularization for each of the filter banks. This gives a feature vector with a total of 36 features, 4 CSP filters \times 9 filter banks, for each trial. Third, an elastic-net logistic regression classifier was trained, with a penalty $\alpha = 0.95$.

Finally, the trained classifier was applied to the test set through cross-validation.

5.3 Riemannian Geometry (RG)

The implementation of the RG used in this thesis is called Tangent Space (TS) followed by logistic regression (TS), TSLR for short. The following steps were applied: Same preprocessing as the other methods except bandpass filtering between 4 Hz and 30 Hz. The covariance matrices were computed and mapped into the Riemannian manifold using the pyRiemann software [9, 10]. Then the matrices were projected onto the tangent space. Logistic regression was used as the classifier, same as for FBCSP.

5.4 Convolutional neural networks

5.4.1 EEGNet

EEGNet is a compact CNN architecture introduced by Lawhern et al. [34]. It is intended for EEG-based BCIs, with the aim of being applicable across several different BCI paradigms, working well with limited data, and producing neurophysiologically interpretable features. See Figure 5.3 for visualization of the architecture of EEGNet. The network learns frequency filters through temporal convolution first. Then, in the middle column, frequency-specific spatial

filters are learned by performing depthwise convolution connected to each individual feature map. The optimal mix of the feature maps together is learned in the fourth column.

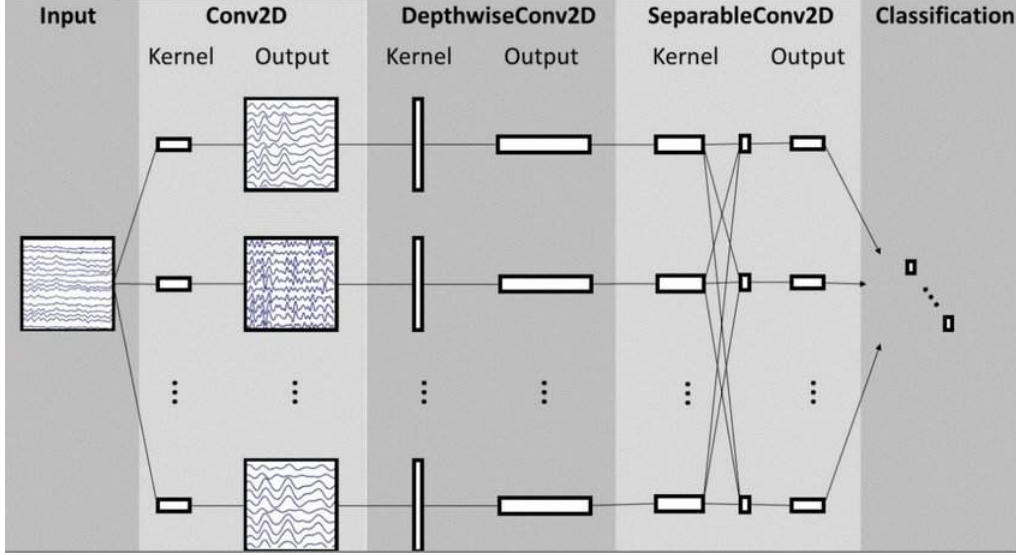


Figure 5.3: Visualization of the EEGNet architecture. [34]

The EEGNet-8,2 version was used in the analysis, where 8 and 2 denote the number of temporal and spatial filters, respectively, to be learned. The temporal kernel length was set to 32 samples, to account for the data being high-pass filtered at 4 Hz. The implemented model was fit using the Adam optimizer, with default parameters, minimizing the categorical cross-entropy loss function. The drop-out rate was set to 0.5, due to the limited training data. The maximum number of training iterations (epochs) was set to 500, and early stopping was enabled, saving the model weights which produced the lowest validation set loss.

5.4.2 DeepConvNet

As described by [66], the deep ConvNet consists of four convolution-max-pooling blocks. The first block is specially designed to handle EEG input. The three following blocks are standard convolution max-pooling layers and a dense softmax classification layer. The first convolutional block is split into two layers for better handling of a large number of input channels, i.e., one input channel per electrode. In the first layer, each filter performs a convolution over time. In the second

layer, each filter performs spatial filtering with weights for all possible pairs of electrodes and filters of the preceding temporal convolution. There is no activation function in between the two layers.

5.4.3 ShallowConvNet

the FBCSP pipeline inspired the ShallowConvNet [66], which is specifically tailored to decode band power features. The transformations performed by FBCSP are similar to the transformations of the shallow ConvNet. Specifically, the first two layers of the shallowConvNet work the same way as in the deep ConvNet, performing temporal convolution and spatial filtering. These steps are the same as the bandpass and filter steps of FBCSP. The shallow ConvNet does however have a larger kernel size than the deep ConvNet, allowing a larger transformation range in this layer. The temporal convolution and the spatial filtering are followed by a squaring nonlinearity, a mean pooling layer, and a logarithmic activation function. These steps correspond to the computation of trial log-variance in FBCSP. Shallow ConvNet embeds all the computational steps in a single network, in contrast to FBCSP, allowing all steps to be optimized jointly. Also, the shallow ConvNet can learn a temporal structure of the band power changes within the trial, due to having several pooling regions within one trial.

5.5 Channel selection

Both manual selection and automatic selection of channels were employed.

In the manual selection, all 8 neighboring electrodes of both C3 and C4 were selected, including C3 and C4 themselves. They were selected based on the literature review that has been performed in this study, which revealed that these channels are located on the sensory-motor cortex, where distinctive activity when performing/imagining different hand movements can be expected.

In addition, an automatic channel selection was made, based on a Riemannian geometry criterion. For each class, a centroid is estimated, and the channel selection is based on the maximization of the distance

between centroids. This is done by a backward elimination where the electrode that carries the less distance is removed from the subset at each iteration [8].

5.6 Subject handling

Inter- or intra-subject classification has an impact on the performance. Models trained on the data of a single subject (intra-subject) have less variability to account for and often lead to higher performances. However, the data available for such models is limited. With multiple subjects included (inter-subject), the model sees more data. This study is limited to intra-subject classification.

5.7 Validation procedure

The validation procedure can impact the performance. Using different subjects for training and testing may lead to lower performance, but is applicable to scenarios in real life. In the experiments of this thesis, Kfold cross-validation was used, where the folds comprised of the various runs. So for the motor imagery case, with 4 runs per subject, the number of folds was 4. When motor execution and imagery were combined, the number of folds was 6, i.e. reflecting the total number of runs. The random state was kept the same for all experiments to ensure a proper comparison.

5.8 Performance measures

For a classification algorithm, the most basic performance measure is accuracy. It is also the most widely used evaluation criteria in BCI research. The classes should be balanced when using this metric, meaning there should be the same number of samples for each class. It is also important to note that the accuracy of a random classifier is already 100% divided by the number class. If there are e.g. 2 classes, there is a 50% chance of correct classification, given balanced classes. Further exploration is required if the accuracy score is lower than this limit [67].

When the classes are unbalanced, or the classifier is biased, a confusion matrix (including sensitivity, specificity, or precision) or the Kappa metric can serve as more informative alternatives. The area under the curve (AUC) and receiver operating characteristic (ROC) are often used when the classification depends on a continuous parameter.

Generally, the performance of a classifier is computed offline on data that has been pre-recorded. For evaluation, some of the data should be set aside, and not be included in the training. Performance may be overrated if measures are estimated through cross-validation on training data [39].

6 Experiments and results

This chapter presents details about all the conducted experiments and their results. A comparison of employed traditional and state-of-the-art methods is made.

The chapter is split into two sections. Section 6.1 describes the experiments. Section 6.2 provides the results.

To investigate the effect of hand-dominance, the right-hand grasps were separated from the left-hand grasps during the experiments, making each of them a binary classification problem. The number of class samples per subject was thereby reduced from 160 (4 classes \times 10 trials \times 4 runs) to 80 (2 classes \times 10 trials \times 4 runs) in the motor imagery case.

The different variations that were tested included:

1. Left hand vs right hand, where all left-hand grasps were combined and marked as LH, and all right-hand grasps were combined and marked as RH. This will from now on be referred to as the LH-RH case.
2. Only left-hand classes included, divided into two separate classes of precision grasp and power grasp. From now on referred to as the LH-LH case.
3. Only right-hand classes included, divided into two separate classes of precision grasp and power grasp. From now on referred to as the RH-RH case.
4. All four classes included, none of them combined. From now on referred to as the 4-class case.

6.1 Experiments

The following experiments were conducted for both left-hand and right-hand grasps, using all the five models introduced in chapter 5 - FBCSP, TSLR, EEGNet, ShallowConvNet, and DeepConvNet.

1. Data from BCI competition IV 2a was classified, to compare results to Lawhern et al. [34], and verify that the algorithms were implemented correctly.
2. Motor imagery data for all subjects, cross-validated on every run. This will be referred to as the baseline experiment.
3. Augmented motor imagery data for all subjects, cross-validated on every run, using sliding window approaches (see section 5.1.3).

4. Augmented motor imagery data for all subjects, cross-validated on every run, using downsampling approach (see section 5.1.3).
5. Motor imagery and executory data for all subjects, cross-validated on every run.
6. Manual channel selection before feature extraction and/or classification.
7. Riemannian automatic channel selection algorithm before feature extraction and/or classification.

The software and hardware used for these experiments are:

- Programming language: Python3
- Signal processing library: MNE-python 0.23.0.
- Traditional baselines: MNE-python 0.23.0 and scikit-learn 0.24.
- Deep learning library: Keras and TensorFlow 2.
- Hardware: Nvidia RTX3090 GPU.

6.2 Results

The reproduction of the results from Lawhern et. al [34] can be seen in Figure 6.1. The hyperparameters and preprocessing methods were kept the same, and the plots were produced to verify that all algorithms were implemented correctly. Tangent space (TSLR) was not used in the compared study but achieved satisfactory results when set side by side with the other models. The accuracy scores are corresponding to those gained by [34], with some expected deviance, presumably due to randomness in folds.

The results of the remaining experiments are presented in tables 6.1-6.4. For simplicity, only the best performing augmentation technique has been included. This was sliding window augmentation with an overlap of 0.1s, providing a five times increase in the amount of data.

The results of the LH-RH classification problem are summarized in Table 6.1. The accuracies are averaged across all folds and all subjects. As expected, due to neural networks achieving better performance

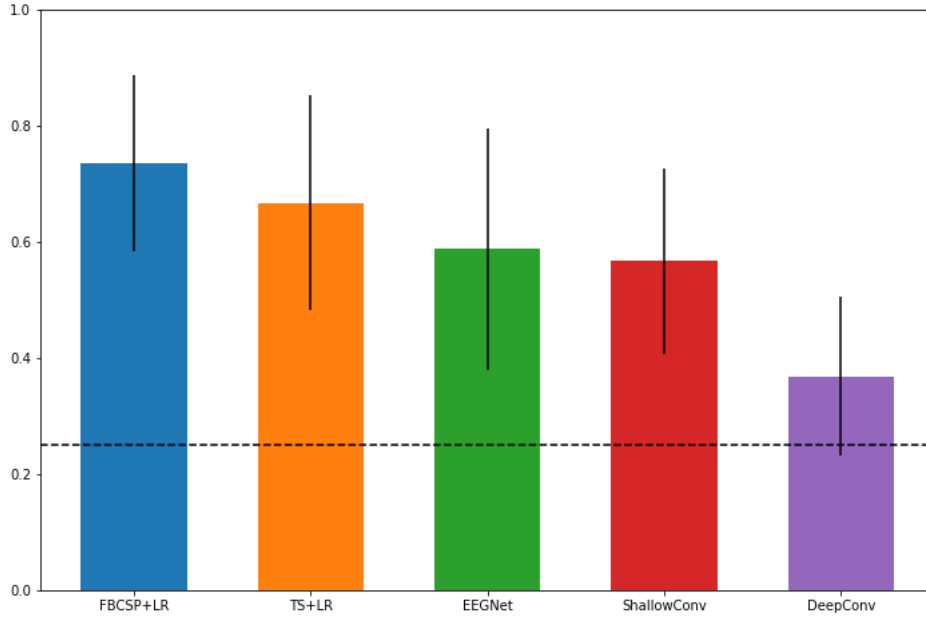


Figure 6.1: Accuracy of implemented algorithms for 4-class problem using BCIC 2a dataset, averaged over all folds and all subjects.

with more training data, sliding window augmentation and adding executory data to the imagery enhances the performance of EEGNet and ShallowConvNet. Interestingly, it does not affect the performance of DeepConvNet. This could be due to the amount of training data still being too small for the intended use of this network. The accuracies of FBCSP are decreasing with this increase in data, while the results of TSLR are approximately the same. Manual channel selection does not stand out with regards to performance, achieving some improvement in FBCSP. Riemann channel selection, on the other hand, provides an improvement in performance for all models, compared to experiments with motor imagery data only. The average accuracy of FBCSP is increased by 7.19 percentage points, due to this selection algorithm.

The results of the LH-LH and RH-RH classification problems are summarized in Tables 6.2 and 6.3, respectively. RH-RH has poorer performance than LH-LH when only imagery data is included. Interestingly, adding motor executory data achieves an increase of up to 4.95 percentage points for the conventional methods in the RH-RH case, surpassing LH-LH, which in fact has a decrease in performance.

The average accuracies are in general very close to random chance, except for Riemann channel selection experiments, which increase the

Table 6.1: LH-RH case: Accuracies averaged accross all subjects and all folds. Best performing experiment marked in bold for each model.

Experiment	FBCSP	TSLR	EEGNet	ShallowConvNet	DeepConvNet
Motor imagery data only	60.99	61.35	54.90	50.89	50.47
Motor imagery + Motor executory	59.65	60.26	57.75	56.45	51.55
Sliding window augmentation	58.16	61.53	58.74	55.44	50.95
Manual channel selection (18 chns)	62.50	60.47	53.39	52.19	48.44
Riemann channel selection (16 chns)	60.83	61.35	55.94	57.19	51.46
Riemann channel selection (8 chns)	68.18	68.59	59.06	55.78	51.30

Table 6.2: LH-LH case: Accuracies averaged accross all subjects and all folds. Best performing experiment marked in bold for each model.

Experiment	FBCSP	TSLR	EEGNet	ShallowConvNet	DeepConvNet
Motor imagery data only	54.17	56.04	53.85	54.48	49.69
Motor imagery + Motor executory	53.86	55.54	55.39	55.33	53.65
Sliding window augmentation	52.48	55.25	54.12	54.60	50.19
Manual channel selection (18 chns)	53.44	49.69	53.65	52.60	50.42
Riemann channel selection (16 chns)	59.27	60.52	53.02	54.69	52.60
Riemann channel selection (8 chns)	60.63	60.31	55.00	57.40	52.40

performance by 11.56 percentage points for the best performing model, compared to the baseline experiment.

Due to the promising results of Riemann channel selection performance, especially with 8 channels, this experiment will be further reviewed by analyzing the performance of the individual subjects. The results are presented in Tables 6.5, 6.6, 6.7, and 6.8.

Riemann geometry and filterbank CSP outperform all convolutional neural networks for most subjects. There is high variability among the subjects. Five out of nine subjects reach accuracy levels above the mentioned threshold (70%) for LH/RH classification. Based on the literature it was to be expected that the majority of the participants should reach such levels.

Table 6.3: RH-RH case: Accuracies averaged accross all subjects and all folds. Best performing experiment marked in bold for each model.

Experiment	FBCSP	TSLR	EEGNet	ShallowConvNet	DeepConvNet
Motor imagery data only	53.33	52.50	53.12	53.85	51.56
Motor imagery + Motor executory	57.59	57.45	54.48	56.25	49.34
Sliding window augmentation	53.63	53.98	53.67	54.02	50.71
Manual channel selection (18 chns)	52.50	53.75	53.65	55.31	52.19
Riemann channel selection (16 chns)	60.83	61.35	55.94	57.19	51.46
Riemann channel selection (8 chns)	63.23	64.06	57.40	57.40	53.33

Table 6.4: 4-class case: Accuracies averaged accross all subjects and all folds. Best performing experiment marked in bold for each model.

Experiment	FBCSP	TSLR	EEGNet	ShallowConvNet	DeepConvNet
Motor imagery data only	30.99	32.92	29.58	26.88	26.09
Motor imagery + Motor executory	30.24	31.80	31.23	28.44	27.12
Sliding window augmentation	30.54	33.57	31.06	31.59	26.39
Manual channel selection (18 chns)	31.46	32.08	28.59	27.34	26.61
Riemann channel selection (16 chns)	38.02	40.63	30.57	29.74	25.68
Riemann channel selection (8 chns)	37.50	37.76	31.25	30.52	25.73

Table 6.5: LH-RH case: Accuracies of individual all subjects averaged over all folds. Accuracies above 70% are marked in bold.

Subj.	FBCSP	TSLR	EEGNet	ShallowConvNet	DeepConvNet
1	85.63	80.63	78.13	62.50	57.50
2	62.50	70.00	58.75	58.75	54.37
3	70.00/71.25	71.25/77.5	65.00/58.75	57.50/58.75	58.75/51.25
4	75.63/61.25/69.38	66.25/65.63/70.00	66.88/51.88/63.75	53.75/54.38/60.63	47.50/46.87/50.63
5	73.13	73.13	57.50	53.75	45.00
6	57.50	56.88	53.13	61.87	55.00
7	66.88	58.75	50.00	46.25	46.25
8	60.63	60.00	48.75	46.25	52.50
9	64.38	73.13	56.25	56.88	50.00
Avg	68.18	68.59	59.06	55.78	51.30

Table 6.6: LH-LH case, with Riemann channel selection, 8 channels: Accuracies of individual all subjects averaged over all folds. Accuracies above 70% marked in bold. The multiple scores for subjects 3 and 4 reflects the different sessions.

Subj.	FBCSP	TSLR	EEGNet	ShallowConvNet	DeepConvNet
1	48.75	46.25	47.50	52.50	45.00
2	60.00	50.00	60.00	56.25	50.00
3	57.50/65.00	48.75/67.50	50.00/57.50	53.75/58.75	57.50/55.00
4	56.25/ 71.25 /62.50	58.75/65.00/58.75	56.25/58.75/61.25	58.75/62.50/50.00	57.50/45.00/52.50
5	60.00	70.00	46.25	58.75	50.00
6	61.25	61.25	48.75	56.25	50.00
7	73.75	76.25	66.25	66.25	57.50
8	52.50	53.75	52.50	57.50	50.00
9	58.75	67.50	55.00	57.50	58.75
Avg	60.63	60.31	55.00	57.40	52.40

Table 6.7: RH-RH case, with Riemann channel selection, 8 channels: Accuracies of individual all subjects averaged over all folds. Accuracies above 70% marked in bold. The multiple scores for subjects 3 and 4 reflects the different sessions.

Subj.	FBCSP	TSLR	EEGNet	ShallowConvNet	DeepConvNet
1	65.00	61.25	51.25	53.75	55.00
2	73.75	78.75	72.50	72.50	61.25
3	65.00/ 76.25	66.22/ 78.75	43.75/ 75.00	48.75/58.75	50.00/55.00
4	62.50/53.75/56.25	65.00/55.00/50.00	66.25/58.75/55.00	61.25/45.00/60.00	50.00/47.50/52.50
5	65.00	67.50	50.00	62.50	51.25
6	56.25	60.00	55.00	52.50	53.75
7	62.50	66.25	58.75	58.75	55.00
8	57.50	62.50	50.00	57.50	52.50
9	65.00	57.50	52.50	57.50	56.25
Avg	63.23	64.06	57.40	57.40	53.33

Table 6.8: 4-class case:, with Riemann channel selection, 8 channels: Accuracies of individual all subjects averaged over all folds. In this case, random chance is at 25%. The multiple scores for subjects 3 and 4 reflects the different sessions.

Subj.	FBCSP	TSLR	EEGNet	ShallowConvNet	DeepConvNet
1	43.75	40.00	36.87	30.00	28.75
2	35.00	41.25	46.87	46.25	25.00
3	33.75/41.88	28.75/47.50	30.00/36.25	36.25/35.00	21.88/30.00
4	45.63/35.00/39.38	37.50/43.75/34.38	36.25/30.00/28.75	23.12/36.25/27.50	25.63/24.37/23.12
5	37.50	38.13	26.25	30.63	25.63
6	33.13	35.00	21.25	29.38	23.13
7	35.00	43.75	30.00	36.25	24.37
8	33.13	35.00	23.75	22.50	26.88
9	36.88	37.50	26.87	28.75	25.62
Avg	37.50	37.76	31.25	30.52	25.73

It should however also be noted that subjects 4, 5, and 7 reach the threshold in the LH-LH case, and subjects 2 and 3 reach it for the RH-RH case. It is interesting to see that the same subjects do not reach these levels in both cases, indicating that there is indeed a difference based on the side of the imagined movement.

In the 4-class problem, the chance level is at 25 %, and all the subjects reach accuracies well above this limit. The best performing subject got a score of 47.50%, so it is however quite far from being deployable in a BCI application.

In Figure 6.2, the accuracies for the best performing subjects of the different cases have been plotted, including standard deviation, visualizing the variance between the different folds, i.e. runs. For some of the models the accuracy varies a lot, depending on the run that is being tested.

Overall, TSLR achieves the highest accuracies, followed by FBCSP. Out of the convolutional neural networks, EEG has the best performance, while deepConvNet in most of the experiments gave accuracies close to chance. The performance of shallowConvNet is along the lines of EEGNet.

The individual results of all the subjects for all experiments can be found in appendix A.

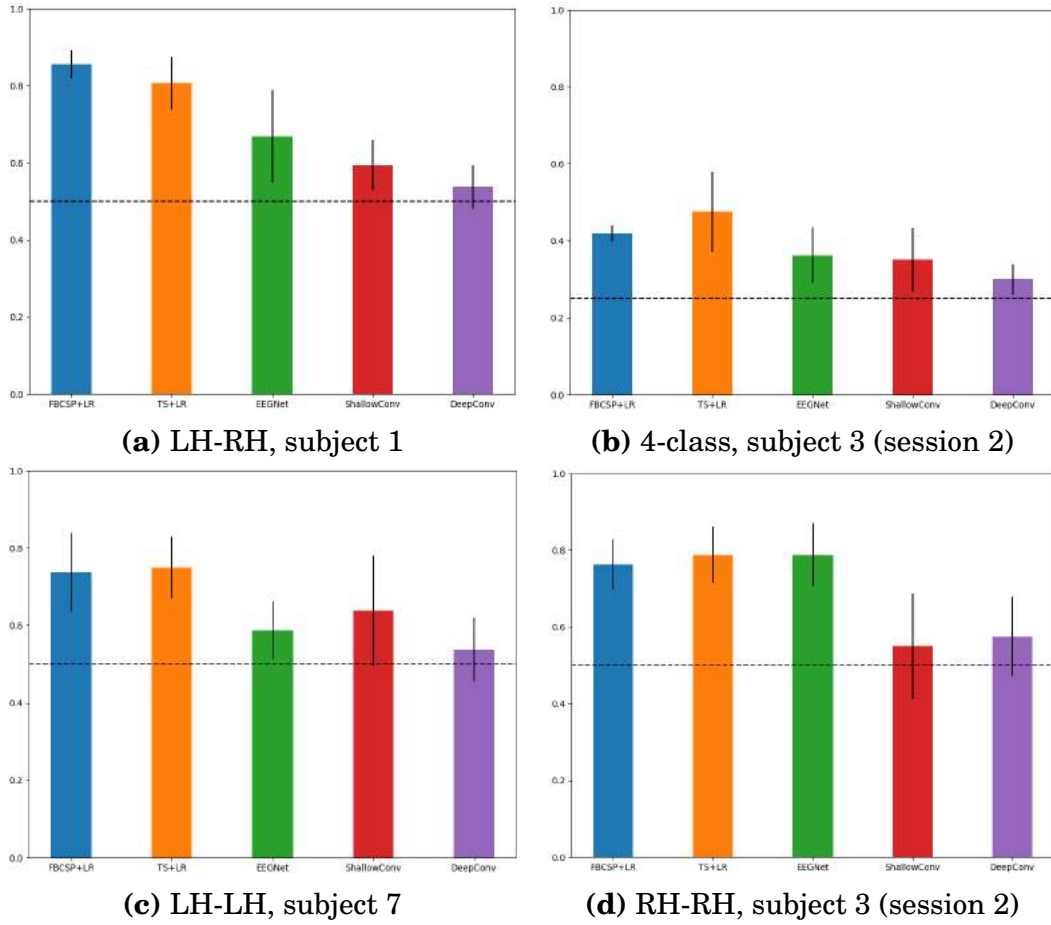


Figure 6.2: Accuracies for best performing subjects of the different cases, all models included. Error bars denote the standard deviation of the folds. The dotted line indicates chance level.

7 Discussion

An evaluation of the results and ethical dilemmas. Research questions are addressed. Recommendations for further research are also given.

The chapter is divided into two sections. Section 7.1 provides some ethical considerations. Section 7.3 presents future work.

One critical limitation of current BCIs applications is the lack of usability. This is mainly due to the small number of available classes for decoding. In this thesis, the aim was to contribute in a direction towards more commands. With that in mind, two research questions were formulated.

1) Does hand-dominance affect the discriminative properties of a set of hand grasps?

The results in chapter 6 show that there is a clear difference in performance with regards to what side the imagery task is performed on. In Table 7.1, the percentage differences between RH-RH and LH-LH classification have been calculated. It should be noted that what side performs better seemingly depends on a variety of factors:

1. The subject performing the task. Subject 2 got 28.75 percentage points better accuracies for RH-RH classification than LH-LH, while e.g. subject 7 got 11.25 percentage points poorer scores when comparing the same cases.
2. The classification model. Subject 9 got better scores for RH-RH imagery when classified with FBCSP, but poorer when using TSLR.
3. The session. For subject 2, which side performs better, varies across the different sessions.

To establish clear trends, a larger number of subjects, trials, and sessions is necessary.

2) To what extent do tasks within the same limb reach decoding accuracies above the required threshold ($\sim 70\%$) for BCI applications?

Five out of the nine subjects reached decoding accuracies above the required threshold for one of the sides. None of them reached it for both LH-LH and RH-RH. The results indicate that same-limb motor imagery has the potential to be utilized in a BCI system, providing additional commands to external devices. It should also be noted that

Table 7.1: RH-RH accuracies subtracted from LH-LH accuracies.

Subj.	FBCSP	TSLR
1	16.25	15.00
2	13.75	28.75
3	7.50/11.25	17.5/11.25
4	6.25/-17.5/-6.25	6.25/-10.00/-8.75
5	5.00	-2.50
6	-5.00	-1.25
7	-11.25	-10.00
8	5.00	8.75
9	6.25	-10.00
Avg	2.6	3,75

when all four classes are considered, the accuracy drops significantly. The four-class system does not pass the minimum threshold, hence more research on the topic is required to achieve satisfactory results.

It is also clear that differences in subject-wise performance is a challenge. In [35] 30% of the subjects were not able to achieve more than 70% decoding accuracy when using an MI-based BCI and approximately 15% showed insufficient decoding accuracy when using ERP-based and SSVEP-based BCIs. The users did however tend to prefer MI to ERP or SSVEP based systems [37]. BCI illiteracy is a proposed condition wherein users of BCI technology fail to reach proficiency in using it within a standard training period [50]. This is a challenge in MI BCI systems, as it means that not everyone can use them. However if successful, users can control a device without eye strain, as is the case for the other paradigms. The subjects that did not achieve accuracies above the threshold in any of the experiments could be suffering from BCI-illiteracy. This applies to two of the subjects, i.e. 22%. It would however be interesting to see if performance could be enhanced if feedback was given during the collection of data.

There is a lack of understanding of the relationship between performance within BCIs and the neuroanatomic state of a user. MI BCIs rely heavily on the user's ability to consciously generate the required signals [50]. More research is needed to understand how these neurological factors affect the performance of MI BCIs in order to understand how they could possibly be exploited to improve

performance.

The performance also varies within trials, runs, and sessions. The classification accuracy is usually at its peak around the chosen window segment in this study, i.e. 0.5 to 2.5. In later stages of the trials, the classification accuracy often decreases. This could be caused by the subject losing concentration towards the end of the task. When collecting data for this study, it was commented that especially the motor imagery runs were tiring, compared to the executory ones.

The variation between the runs for the best performing subjects is visualized in Figure 7.1. There is no clear tendency as to which run performs better or worse. It is observed that for the LH-RH and RH-RH cases, all runs were above the required threshold, suggesting that the trained classifiers in these cases are quite robust. The highest variation among runs can be seen in 7.1b, also displaying a steady improvement throughout the runs.

7.1 Ethical considerations

As the field of brain-computer interface research grows and the technology in brain-computer interface applications continues to improve, a number of ethical issues have been raised.

A BCI is a software application, sending information to an external device. The transmitted data can potentially fall into the wrong hands. Security is especially critical in BCI technology because BCI captures signals directly from a subject's nervous system. BCIs could e.g. be used to determine a user's health status, which presents a significant privacy risk.

Ethical considerations arise when determining how BCI data should be stored and protected. While much of the discussion around ethical issues related to brain-computer interfaces are still being shaped, privacy and security issues remain premier concerns of today. Should Elon Musk achieve his "symbiosis with artificial intelligence", as mentioned introductory, the ethical considerations will be in a whole new ballgame.

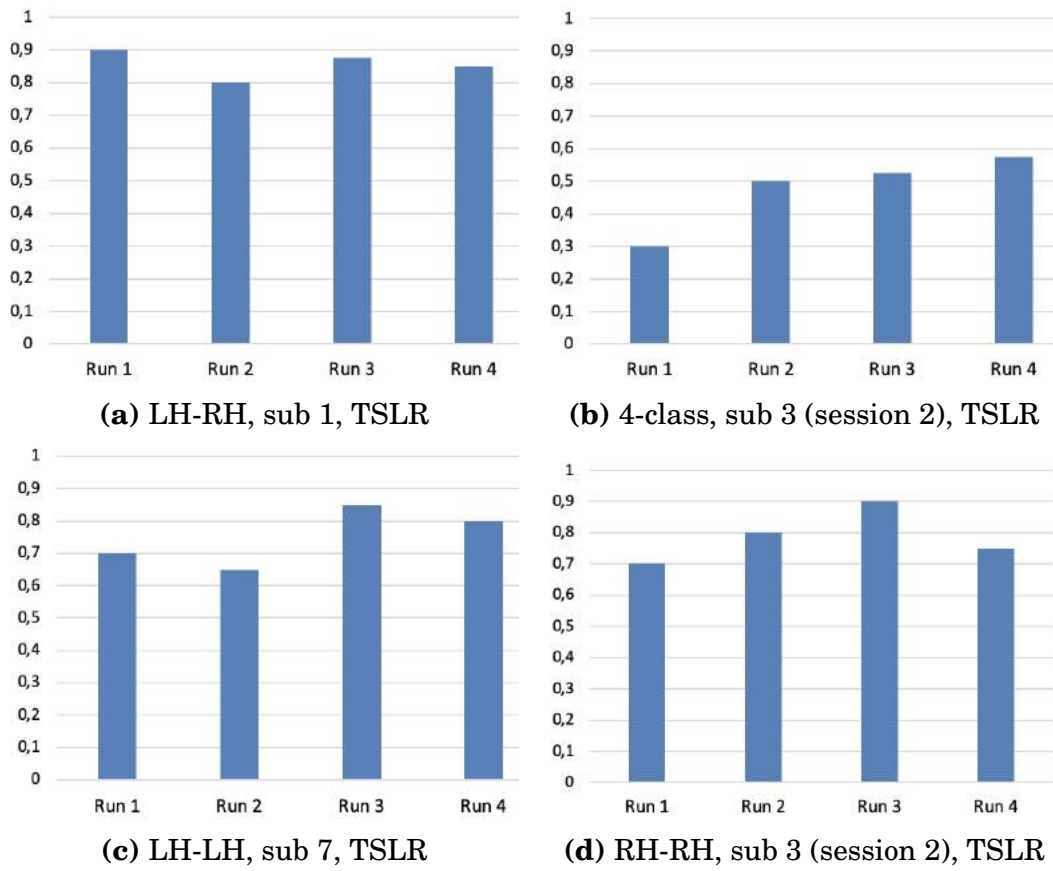


Figure 7.1: Accuracies for best performing subjects of the different cases, with each run used as unseen test data.

7.2 Future work

There are many ways to further explore the collected dataset beyond the scope of this work. Models pre-trained on open relevant datasets can be used for transfer learning, aiming for better initialization and/or regularization. This could perhaps enhance the performance of the neural networks especially. Several other models, feature extraction, and feature selection techniques can be tested to improve performance.

There is a shifting focus in the BCI field from inter-subject analysis to intra-subject analysis. It would be exciting to examine this aspect further, as such a system would require no training from the user, and the amount of available training data would be substantially increased. The session-to-session problem could also be interesting to explore, as two of the subjects in the dataset were recorded for two and three sessions.

Further understanding of the extracted features, would also be helpful upon the investigation of novel classification methods, specifically focused on single-limb classification. Structural and functional differences are known to exist within the cortical sensorimotor networks with respect to the dominant vs. non-dominant hand. The findings in this study indicates that further research is worthwhile.

8 Summary and conclusion

This chapter presents the conclusion of this study by summarizing the results.

This project researched both traditional approaches and convolutional neural networks to classify a privately collected EEG dataset. Through a literary review, a general introduction of the oscillatory activity based brain-computer interfaces was made.

The main objective was to determine whether hand-dominance has an effect when classifying imagery movements within the same limb and to investigate to what extent finer motor tasks on a single limb can reach acceptable performance criteria to pass as additional commands in a BCI. In order to investigate these matters, an EEG dataset with nine right-handed participants was collected. They performed an identical set of grasping tasks with both dominant and non-dominant hand.

To establish a baseline, current state-of-the-art algorithms in traditional machine learning, i.e. FBCSP and Riemannian geometry were implemented and compared to novel, promising, EEG-tailored convolutional neural networks. Different data augmentation and feature selection techniques were explored in various experiments.

One of the experiments, using a Riemann geometry-based channel selection before feature extraction/classification, outperformed the others. Tangent Space logistic regression yielded the highest accuracy scores averaged over all the subjects, namely 68.59% for right-hand/left-hand classification, 64.06% for two different right-hand grasps, and 40.63% for the 4-class problem. FBCSP achieved the highest average for left-hand grasps, with a score of 60.63%. Hence none of the scores averaged across all subjects reached the required accuracy level of 70%. Some of the individual subjects in the study did, however. The best scores were 85.63% for right-hand/left-hand (RH/LH) discrimination, 76.25% for LH/LH grasps, 78.75% for RH/RH grasps, and 46.87% for the 4-class distinction. BCI illiteracy could be the reason why some of the subjects failed to reach accuracy levels above the required minimum to be deployed in a BCI application.

There was a clear tendency on most of the subjects that one of the sides provided higher accuracy decoding levels than the other. As to which side, dominant or non-dominant, was varying across the subjects. The findings in this report do encourage further research on the topic.

A Appendix

The individual results of all the subjects for left-hand/right-hand, left-hand/left-hand grasps and right-hand/right-hand grasps have been included in this appendix.

MOTOR IMAGERY - LH/RH:

Subj.	FBCSP			TSLR			EEGNet			ShallowConvNet			DeepConvNet		
1	76.88			78.75			75.62			55.00			50.00		
2	53.13			58.13			52.50			51.25			48.75		
3	68.75	66.88		60.00	68.13		59.38	58.75		53.75	51.88		48.75	51.87	
4	64.38	55.63	53.75	70.00	61.25	63.13	45.00	46.25	52.50	43.12	48.12	56.25	44.38	53.13	49.38
5	68.75			68.13			60.00			50.00			48.75		
6	66.88			48.75			53.75			50.00			56.25		
7	55.00			51.25			51.25			47.50			49.37		
8	52.50			53.75			50.00			53.75			53.75		
9	49.38			55.00			53.75			50.00			51.25		
Avg	60.99			61.35			54.90			50.89			50.47		

MOTOR IMAGERY - LH/LH:

Subj.	FBCSP			TSLR		EEGNet			ShallowConvNet			DeepConvNet			
1	46.25			56.25		43.75			45.00			55.00			
2	55.00			51.25		57.50			42.50			45.00			
3	50.00	62.50		56.25	58.75		50.00	50.00		61.25	51.25		52.50	46.25	
4	52.50	62.50	53.75	70.00	50.00	68.75	57.50	51.25	51.25	55.00	56.25	53.75	50.00	46.25	48.75
5	53.75			45.00		63.75			50.00			51.25			
6	50.00			46.25		58.75			67.50			45.00			
7	56.25			67.50		56.25			61.25			57.50			
8	50.00			51.25		48.75			57.50			50.00			
9	57.50			51.25		57.50			52.50			48.75			
Avg	54.17			56.04		53.85			54.48			49.69			

MOTOR IMAGERY - RH/RH:

Subj.	FBCSP			TSLR			EEGNet			ShallowConvNet			DeepConvNet		
1	56.25			50.00			47.50			45.00			47.50		
2	53.75			51.25			61.25			71.25			56.25		
3	53.75	60.00		45.00	67.50		41.25	70.00		56.25	60.00		50.00	55.00	
4	66.25	52.50	45.00	46.25	56.25	43.75	47.50	48.75	55.00	56.25	53.75	51.25	53.75	52.50	51.25
5	55.00			52.50			46.25			46.25			40.00		
6	38.75			43.75			56.25			48.75			52.50		
7	50.00			57.50			52.50			57.50			60.00		
8	55.00			57.50			48.75			46.25			47.50		
9	53.75			58.75			62.50			53.75			52.50		
Avg	53.33			52.50			53.12			53.85			51.56		

MOTOR IMAGERY AND EXECUTION - LH/RH:

Subj.	FBCSP			TSLR			EEGNet			ShallowConvNet			DeepConvNet		
1	72.00			81.50			71.00			62.00			52.50		
2	50.61			51.87			49.75			53.12			49.00		
3	59.17	68.75		63.33	73.75		51.67	75.83		50.00	61.67		50.83	54.17	
4	67.50	52.92	56.67	63.33	52.50	54.17	53.33	51.67	55.42	61.25	54.17	58.33	48.33	50.00	52.08
5	57.50			62.50			52.50			47.92			50.00		
6	64.58			52.50			54.58			56.67			51.67		
7	61.53			65.75			65.28			60.65			52.28		
8	54.58			54.17			60.83			58.33			53.75		
9	52.08			51.25			53.33			54.17			54.17		
Avg	59.65			60.26			57.75			56.45			51.55		

MOTOR IMAGERY AND EXECUTION - LH/LH:

Subj.	FBCSP			TSLR			EEGNet			ShallowConvNet			DeepConvNet		
1	43.00			51.00			58.00			50.00			46.00		
2	51.67			55.00			51.67			46.67			54.17		
3	49.17	62.50		49.17	58.33		52.50	58.33		54.17	53.33		56.67	56.67	
4	53.33	52.50	55.83	68.33	52.50	50.83	57.50	59.17	53.33	45.00	44.17	65.00	51.67	52.50	52.50
5	55.00			64.17			59.17			64.17			49.17		
6	48.33			40.83			55.00			61.67			52.50		
7	67.37			71.36			55.48			73.11			64.82		
8	51.67			53.33			49.17			55.00			55.00		
9	54.17			50.83			55.83			50.83			50.83		
Avg	53.86			55.54			55.39			55.33			53.65		

MOTOR IMAGERY AND EXECUTION - RH/RH:

Subj.	FBCSP			TSLR		EEGNet			ShallowConvNet			DeepConvNet			
1	55.00			48.00		51.00			53.00			60.00			
2	63.16			65.61		70.53			72.24			50.48			
3	58.33	71.67		50.00	60.83		41.67	60.83		44.17	59.17		44.17	53.33	
4	57.50	60.83	57.50	61.67	51.67	60.83	65.00	49.17	49.17	55.00	58.33	54.17	49.17	48.33	48.33
5	50.83			61.67		55.83			63.33			50.83			
6	48.33			50.00		51.67			45.00			40.83			
7	66.67			67.50		63.33			60.00			49.17			
8	46.67			46.67		48.33			54.17			45.00			
9	54.17			63.33		46.67			55.83			54.17			
Avg	57.59			57.45		54.48			56.25			49.34			

MOTOR IMAGERY - LH/RH. (Window slide augmentation)

	FBCSP				TSLR			EEGNet			ShallowConvNet			DeepConvNet		
1	70.50				76.25			75.00			67.75			50.87		
2	48.88				61.50			53.88			55.75			52.50		
3	63.50	64.25		60.13	67.75		60.00	70.00		54.13	56.13		53.50	54.13		
4	61.13	54.13	55.63	66.00	59.88	62.38	66.50	52.00	60.25	58.62	49.00	56.00	48.25	48.88	47.00	
5	65.50				66.13			52.50			51.50			51.12		
6	59.25				47.13			51.00			48.50			46.75		
7	50.38				56.25			56.13			57.25			53.38		
8	54.25				55.88			56.00			55.25			54.38		
9	50.50				59.13			51.63			55.38			50.62		
Avg	58.16				61.53			58.74			55.44			50.95		

MOTOR IMAGERY - LH/LH. (Window slide augmentation)

	FBCSP			TSLR			EEGNet			ShallowConvNet			DeepConvNet		
1	46.00			58.00			54.00			58.00			44.75		
2	51.50			45.50			54.00			45.25			48.25		
3	52.00	58.25		49.00	64.75		57.75	56.75		54.50	56.50		55.25	49.25	
4	54.75	47.25	55.50	59.25	60.25	58.50	56.50	56.50	50.00	58.50	45.00	54.25	51.00	48.25	50.00
5	53.00			50.25			50.50			54.00			49.00		
6	54.00			51.75			54.25			56.50			54.00		
7	55.00			60.00			55.25			64.75			56.75		
8	50.75			59.50			51.25			54.25			48.75		
9	51.75			46.25			52.75			53.75			47.00		
Avg	52.48			55.25			54.12			54.60			50.19		

MOTOR IMAGERY - RH/RH. (Window slide augmentation)

	FBCSP			TSLR			EEGNet			ShallowConvNet			DeepConvNet		
1	52.00			57.00			53.25			54.25			48.50		
2	53.25			47.75			64.25			62.25			49.25		
3	59.00	59.25		48.75	70.75		55.25	70.25		53.50	59.25		51.00	52.75	
4	59.75	56.00	49.75	50.50	54.00	46.75	59.25	47.00	52.25	53.00	56.00	50.25	52.50	48.25	56.50
5	53.75			57.25			54.50			58.75			52.00		
6	44.50			45.50			47.00			45.25			49.50		
7	53.50			58.25			50.75			52.75			51.00		
8	48.75			52.50			42.75			44.75			51.00		
9	54.00			58.75			47.50			58.25			46.25		
Avg	53.63			53.98			53.67			54.02			50.71		

MOTOR IMAGERY - LH/RH. Manual channel selection (18 chs):

Subj.	FBCSP			TSLR			EEGNet			ShallowConvNet			DeepConvNet		
1	82.50			85.00			70.63			65.00			53.13		
2	55.63			57.50			48.75			48.75			43.75		
3	65.00	63.75		64.38	56.25		47.50	50.62		50.62	50.62		45.00	50.62	
4	68.13	58.75	62.50	65.63	60.00	58.75	53.13	50.63	53.75	51.87	53.75	52.50	50.00	50.62	48.75
5	70.63			65.63			57.50			42.50			48.13		
6	56.25			48.13			51.87			50.63			49.37		
7	61.88			56.25			49.37			48.75			45.62		
8	51.25			54.38			55.63			53.75			51.25		
9	53.75			53.75			51.25			57.50			45.00		
Avg	62.50			60.47			53.39			52.19			48.44		

MOTOR IMAGERY - LH/LH. Manual channel selection (18 chs):

Subj.	FBCSP			TSLR			EEGNet			ShallowConvNet			DeepConvNet		
1	37.50			60.00			57.50			47.50			45.00		
2	47.50			40.00			48.75			46.25			45.00		
3	60.00	52.50		53.75	42.50		50.00	57.50		62.50	53.75		48.75	57.50	
4	56.25	58.75	62.50	38.75	50.00	60.00	57.50	47.50	58.75	56.25	48.75	51.25	48.75	45.00	52.50
5	52.50			42.50			45.00			53.75			56.25		
6	57.50			57.50			52.50			56.25			48.75		
7	45.00			48.75			57.50			57.50			61.25		
8	52.50			55.00			55.00			52.50			43.75		
9	58.75			47.50			56.25			45.00			52.50		
Avg	53.44			49.69			53.65			52.60			50.42		

MOTOR IMAGERY - RH/RH. Manual channel selection (18 chs):

Subj.	FBCSP			TSLR			EEGNet			ShallowConvNet			DeepConvNet		
1	56.25			51.25			46.25			55.00			48.75		
2	46.25			42.50			62.50			56.25			61.25		
3	52.50	63.75		58.75	76.25		56.25	62.50		48.75	60.00		53.75	67.50	
4	50.00	53.75	50.00	48.75	48.75	53.75	57.50	48.75	51.25	63.75	50.00	57.50	52.50	48.75	46.25
5	55.00			47.50			48.75			55.00			45.00		
6	47.50			56.25			51.25			53.75			51.25		
7	53.75			61.25			60.00			53.75			52.50		
8	41.25			37.50			47.50			57.50			52.50		
9	60.00			62.50			51.25			52.50			46.25		
Avg	52.50			53.75			53.65			55.31			52.19		

MOTOR IMAGERY - LH/RH. Riemann channel selection (16 chs):

Subj.	FBCSP			TSLR			EEGNet			ShallowConvNet			DeepConvNet		
1	81.25			80.00			68.13			65.63			49.38		
2	53.75			66.25			56.88			50.63			48.75		
3	65.00	79.38		65.63	83.75		58.75	68.13		55.00	59.38		56.88	55.63	
4	66.88	68.75	61.88	65.00	65.63	66.88	64.38	48.75	52.50	52.50	48.75	57.50	55.00	46.88	47.50
5	73.75			73.75			52.50			51.25			51.88		
6	63.13			60.00			50.63			53.75			51.25		
7	64.38			66.88			53.13			46.25			42.50		
8	61.88			61.25			53.75			55.00			51.25		
9	63.13			62.50			52.50			55.00			50.63		
Avg	66.93			68.13			56.67			54.22			50.63		

MOTOR IMAGERY - LH/LH. Riemann channel selection (16 chs):

Subj.	FBCSP			TSLR			EEGNet			ShallowConvNet			DeepConvNet		
1	47.50			53.75			45.00			55.00			52.50		
2	61.25			63.75			48.75			47.50			46.25		
3	56.25	67.50		52.50	68.75		53.75	61.25		53.75	55.00		58.75	55.00	
4	55.00	76.25	58.75	66.25	70.00	57.50	61.25	52.50	43.75	45.00	50.00	51.25	57.50	57.50	55.00
5	57.50			60.00			56.25			61.25			51.25		
6	52.50			50.00			53.75			60.00			47.50		
7	63.75			73.75			51.25			66.25			56.25		
8	48.75			48.75			46.25			61.25			43.75		
9	66.25			61.25			62.50			50.00			50.00		
Avg	59.27			60.52			53.02			54.69			52.60		

MOTOR IMAGERY - RH/RH. Riemann channel selection (16 chs):

Subj.	FBCSP			TSLR			EEGNet			ShallowConvNet			DeepConvNet		
1	62.50			71.25			51.25			66.25			43.75		
2	76.25			76.25			85.00			81.25			55.00		
3	57.50	71.25		52.50	67.50		55.00	53.75		47.50	55.00		50.00	61.25	
4	66.25	53.75	53.75	55.00	56.25	40.00	63.75	45.00	48.75	65.00	58.75	53.75	52.50	51.25	48.75
5	56.25			67.50			57.50			55.00			53.75		
6	61.25			55.00			53.75			45.00			52.50		
7	61.25			67.50			65.00			56.25			55.00		
8	51.25			68.75			40.00			50.00			48.75		
9	58.75			58.75			52.50			52.50			45.00		
Avg	60.83			61.35			55.94			57.19			51.46		

MOTOR IMAGERY - LH/RH. Riemann channel selection (8 chs):

Subj.	FBCSP			TSLR			EEGNet			ShallowConvNet			DeepConvNet		
1	85.63			80.63			78.13			62.50			57.50		
2	62.50			70.00			58.75			58.75			54.37		
3	70.00	71.25		71.25	77.50		65.00	58.75		57.50	56.88		58.75	51.25	
4	75.63	61.25	69.38	66.25	65.63	70.00	66.88	51.88	63.75	53.75	54.38	60.63	47.50	46.87	50.63
5	73.13			73.13			57.50			53.75			45.00		
6	57.50			56.88			53.13			61.87			55.00		
7	66.88			58.75			50.00			46.25			46.25		
8	60.63			60.00			48.75			46.25			52.50		
9	64.38			73.13			56.25			56.88			50.00		
Avg	68.18			68.59			59.06			55.78			51.30		

MOTOR IMAGERY - LH/LH. Riemann channel selection (8 chs):

Subj.	FBCSP			TSLR			EEGNet			ShallowConvNet			DeepConvNet		
1	48.75			46.25			47.50			52.50			45.00		
2	60.00			50.00			60.00			56.25			50.00		
3	57.50	65.00		48.75	67.50		50.00	57.50		53.75	58.75		57.50	55.00	
4	56.25	71.25	62.50	58.75	65.00	58.75	56.25	58.75	61.25	58.75	62.50	50.00	57.50	45.00	52.50
5	60.00			70.00			46.25			58.75			50.00		
6	61.25			61.25			48.75			56.25			50.00		
7	73.75			76.25			66.25			66.25			57.50		
8	52.50			53.75			52.50			57.50			50.00		
9	58.75			67.50			55.00			57.50			58.75		
Avg	60.63			60.31			55.00			57.40			52.40		

MOTOR IMAGERY - RH/RH. Riemann channel selection (8 chs):

Subj.	FBCSP			TSLR			EEGNet			ShallowConvNet			DeepConvNet		
1	65.00			61.25			51.25			53.75			55.00		
2	73.75			78.75			72.50			72.50			61.25		
3	65.00	76.25		66.25	78.75		43.75	75.00		48.75	58.75		50.00	55.00	
4	62.50	53.75	56.25	65.00	55.00	50.00	66.25	58.75	55.00	61.25	45.00	60.00	50.00	47.50	52.50
5	65.00			67.50			50.00			62.50			51.25		
6	56.25			60.00			55.00			52.50			53.75		
7	62.50			66.25			58.75			58.75			55.00		
8	57.50			62.50			50.00			57.50			52.50		
9	65.00			57.50			52.50			57.50			56.25		
Avg	63.23			64.06			57.40			57.40			53.33		

Bibliography

- [1] Priyanka A. Abhang, Bharti W. Gawali, and Suresh C. Mehrotra. “Chapter 2 - Technological Basics of EEG Recording and Operation of Apparatus.” In: *Introduction to EEG- and Speech-Based Emotion Recognition*. Ed. by Priyanka A. Abhang, Bharti W. Gawali, and Suresh C. Mehrotra. Academic Press, Jan. 1, 2016, pp. 19–50. ISBN: 978-0-12-804490-2. DOI: 10 . 1016 / B978 - 0 - 12 - 804490 - 2 . 00002 - 6. URL: [https : / / www . sciencedirect . com / science / article / pii / B9780128044902000026](https://www.sciencedirect.com/science/article/pii/B9780128044902000026) (visited on 06/13/2021).
- [2] Reza Abiri et al. “A comprehensive review of EEG-based brain–computer interface paradigms.” In: *Journal of Neural Engineering* 16.1 (Jan. 2019). Publisher: IOP Publishing, p. 011001. ISSN: 1741-2552. DOI: 10 . 1088 / 1741 - 2552 / aaf12e. URL: [https : / / doi . org / 10 . 1088 / 1741 - 2552 / aaf12e](https://doi.org/10.1088/1741-2552/aaf12e) (visited on 02/25/2021).
- [3] Aiqin Sun, Binghui Fan, and Chaochuan Jia. “Motor imagery EEG-based online control system for upper artificial limb.” In: *Proceedings 2011 International Conference on Transportation, Mechanical, and Electrical Engineering (TMEE)*. Proceedings 2011 International Conference on Transportation, Mechanical, and Electrical Engineering (TMEE). Dec. 2011, pp. 1646–1649. DOI: 10.1109/TMEE.2011.6199526.
- [4] Kai Ang et al. *Filter Bank Common Spatial Pattern (FBCSP) in brain-computer interface*. Journal Abbreviation: Proceedings of the International Joint Conference on Neural Networks Pages: 2397 Publication Title: Proceedings of the International Joint

- Conference on Neural Networks. July 8, 2008. 2390 pp. DOI: 10.1109/IJCNN.2008.4634130.
- [5] Kai Keng Ang et al. “Filter Bank Common Spatial Pattern Algorithm on BCI Competition IV Datasets 2a and 2b.” In: *Frontiers in Neuroscience* 6 (2012). Publisher: Frontiers. ISSN: 1662-453X. DOI: 10.3389/fnins.2012.00039. URL: <https://www.frontiersin.org/articles/10.3389/fnins.2012.00039/full#B1> (visited on 06/09/2021).
 - [6] Mahnaz Arvaneh et al. “Optimizing the Channel Selection and Classification Accuracy in EEG-Based BCI.” In: *Biomedical Engineering, IEEE Transactions on* 58 (July 1, 2011), pp. 1865–1873. DOI: 10.1109/TBME.2011.2131142.
 - [7] *Bandpower of an EEG signal*. URL: <https://raphaelvallat.com/bandpower.html> (visited on 03/02/2021).
 - [8] Alexandre Barachant. *MEG decoding using Riemannian Geometry and Unsupervised classification*. 2014.
 - [9] Alexandre Barachant et al. “Classification of covariance matrices using a Riemannian-based kernel for BCI applications.” In: *Neurocomputing* 112 (July 2013). Publisher: Elsevier, pp. 172–178. DOI: 10.1016/j.neucom.2012.12.039. URL: <https://hal.archives-ouvertes.fr/hal-00820475> (visited on 06/10/2021).
 - [10] Alexandre Barachant et al. “Multiclass Brain-Computer Interface Classification by Riemannian Geometry.” In: *IEEE Transactions on Biomedical Engineering* 59.4 (Mar. 2012). Publisher: Institute of Electrical and Electronics Engineers, pp. 920–928. DOI: 10.1109/TBME.2011.2172210. URL: <https://hal.archives-ouvertes.fr/hal-00681328> (visited on 06/10/2021).
 - [11] Richard Bellman. *Dynamic Programming*. Google-Books-ID: wd-toPwAACAAJ. Princeton University Press, 1957. 342 pp. ISBN: 978-0-691-07951-6.

- [12] Niels Birbaumer. “Breaking the silence: Brain–computer interfaces (BCI) for communication and motor control.” In: *Psychophysiology* 43.6 (2006). Place: Malden, USA Publisher: Blackwell Publishing Inc, Wiley Subscription Services, Inc, pp. 517–532. ISSN: 0048-5772. DOI: 10.1111/j.1469-8986.2006.00456.x.
- [13] Benjamin Blankertz et al. “Optimizing Spatial filters for Robust EEG Single-Trial Analysis.” In: *IEEE Signal Processing Magazine* 25.1 (2008). Conference Name: IEEE Signal Processing Magazine, pp. 41–56. ISSN: 1558-0792. DOI: 10.1109/MSP.2008.4408441.
- [14] Benjamin Blankertz et al. “The Berlin Brain–Computer Interface: Non-Medical Uses of BCI Technology.” In: *Frontiers in Neuroscience* 4 (Dec. 8, 2010). ISSN: 1662-4548. DOI: 10.3389/fnins.2010.00198. URL: <https://www.ncbi.nlm.nih.gov/pmc/articles/PMC3002462/> (visited on 06/13/2021).
- [15] D. H. Brainard. “The Psychophysics Toolbox.” In: *Spatial Vision* 10.4 (1997), pp. 433–436. ISSN: 0169-1015.
- [16] C Brunner et al. “BCI Competition 2008 – Graz data set A.” In: (2008), p. 6.
- [17] Hohyun Cho et al. “A Step-by-Step Tutorial for a Motor Imagery–Based BCI.” In: Jan. 24, 2018, pp. 445–460.
- [18] Febo Cincotti et al. “Non-invasive brain–computer interface system: Towards its application as assistive technology.” In: *Brain research bulletin* 75.6 (2008). Place: United States Publisher: Elsevier Inc, Elsevier BV, pp. 796–803. ISSN: 0361-9230. DOI: 10.1016/j.brainresbull.2008.01.007.
- [19] Guido Dornhege et al. “Boosting bit rates in noninvasive EEG single-trial classifications by feature combination and multiclass paradigms.” In: *IEEE transactions on bio-medical engineering* 51.6 (June 2004), pp. 993–1002. ISSN: 0018-9294. DOI: 10.1109/TBME.2004.827088.

- [20] Bradley J. Edelman, Bryan Baxter, and Bin He. “EEG Source Imaging Enhances the Decoding of Complex Right-Hand Motor Imagery Tasks.” In: *IEEE transactions on bio-medical engineering* 63.1 (Jan. 2016), pp. 4–14. ISSN: 1558-2531. DOI: 10.1109/TBME.2015.2467312.
- [21] Arvid Frydenlund and Frank Rudzicz. “Emotional Affect Estimation Using Video and EEG Data in Deep Neural Networks.” In: *Advances in Artificial Intelligence*. Ed. by Denilson Barbosa and Evangelos Milios. Lecture Notes in Computer Science. Cham: Springer International Publishing, 2015, pp. 273–280. ISBN: 978-3-319-18356-5. DOI: 10.1007/978-3-319-18356-5_24.
- [22] Sheng Ge, Ruimin Wang, and Dongchuan Yu. “Classification of Four-Class Motor Imagery Employing Single-Channel Electroencephalography.” In: *PLOS ONE* 9.6 (June 20, 2014). Publisher: Public Library of Science, e98019. ISSN: 1932-6203. DOI: 10.1371/journal.pone.0098019. URL: <https://journals.plos.org/plosone/article?id=10.1371/journal.pone.0098019> (visited on 05/18/2021).
- [23] Ary L. Goldberger et al. “PhysioBank, PhysioToolkit, and PhysioNet.” In: *Circulation* 101.23 (June 13, 2000). Publisher: American Heart Association, e215–e220. DOI: 10.1161/01.CIR.101.23.e215. URL: <https://www.ahajournals.org/doi/full/10.1161/01.cir.101.23.e215> (visited on 06/15/2021).
- [24] B Graimann et al. “Visualization of significant ERD/ERS patterns in multichannel EEG and ECoG data.” In: *Clinical Neurophysiology* 113.1 (Jan. 1, 2002), pp. 43–47. ISSN: 1388-2457. DOI: 10.1016/S1388-2457(01)00697-6. URL: <https://www.sciencedirect.com/science/article/pii/S1388245701006976> (visited on 06/09/2021).
- [25] Bernhard Graimann, Brendan Allison, and Gert Pfurtscheller. “Brain–Computer Interfaces: A Gentle Introduction.” In: *Brain-Computer Interfaces: Revolutionizing Human-Computer Interaction*. Ed. by Bernhard Graimann, Gert Pfurtscheller, and Brendan Allison. The Frontiers Collection. Berlin, Heidelberg: Springer, 2010, pp. 1–27. ISBN: 978-3-642-02091-9. DOI: 10.

- 1007/978-3-642-02091-9_1. URL: https://doi.org/10.1007/978-3-642-02091-9_1 (visited on 06/13/2021).
- [26] Alexandre Gramfort et al. "MEG and EEG data analysis with MNE-Python." In: *Frontiers in Neuroscience* 7 (2013). Publisher: Frontiers. ISSN: 1662-453X. DOI: 10.3389/fnins.2013.00267. URL: <https://www.frontiersin.org/articles/10.3389/fnins.2013.00267/full> (visited on 06/09/2021).
- [27] Christoph Guger et al. *Prosthetic Control by an EEG-based Brain-Computer Interface (BCI)*. 1999.
- [28] *Headcap, Headcaps*. URL: <https://www.biosemi.com/headcap.htm> (visited on 05/02/2021).
- [29] Camille Jeunet, B kaoua, and Fabien Lotte. "Advances in User-Training for Mental-Imagery Based BCI Control: Psychological and Cognitive Factors and their Neural Correlates." In: (Feb. 26, 2016).
- [30] Valer Jurcak, Daisuke Tsuzuki, and Ippeita Dan. "10/20, 10/10, and 10/5 systems revisited: Their validity as relative head-surface-based positioning systems." In: *NeuroImage (Orlando, Fla.)* 34.4 (2007). Place: United States Publisher: Elsevier Inc, Elsevier BV, pp. 1600–1611. ISSN: 1053-8119. DOI: 10.1016/j.neuroimage.2006.09.024.
- [31] Jasmin Kevric and Abdulhamit Subasi. "Comparison of signal decomposition methods in classification of EEG signals for motor-imagery BCI system." In: *Biomedical Signal Processing and Control* 31 (Jan. 1, 2017), pp. 398–406. ISSN: 1746-8094. DOI: 10.1016/j.bspc.2016.09.007. URL: <https://www.sciencedirect.com/science/article/pii/S1746809416301331> (visited on 06/13/2021).
- [32] Z. J. Koles. "The quantitative extraction and topographic mapping of the abnormal components in the clinical EEG." In: *Electroencephalography and Clinical Neurophysiology* 79.6 (Dec. 1, 1991), pp. 440–447. ISSN: 0013-4694. DOI: 10.1016/0013-4694(91)90163-X. URL: [https://www.sciencedirect.com/science/article/pii/0013-4694\(91\)90163-X](https://www.sciencedirect.com/science/article/pii/0013-4694(91)90163-X).

- com/science/article/pii/001346949190163X (visited on 06/09/2021).
- [33] A. Kübler et al. “Brain-computer communication: self-regulation of slow cortical potentials for verbal communication.” In: *Archives of Physical Medicine and Rehabilitation* 82.11 (Nov. 2001), pp. 1533–1539. ISSN: 0003-9993. DOI: 10.1053/apmr.2001.26621.
 - [34] Vernon J. Lawhern et al. “EEGNet: A Compact Convolutional Network for EEG-based Brain-Computer Interfaces.” In: *Journal of Neural Engineering* 15.5 (Oct. 1, 2018), p. 056013. ISSN: 1741-2560, 1741-2552. DOI: 10.1088/1741-2552/aace8c. arXiv: 1611.08024. URL: <http://arxiv.org/abs/1611.08024> (visited on 06/10/2021).
 - [35] Min-Ho Lee et al. “EEG dataset and OpenBMI toolbox for three BCI paradigms: an investigation into BCI illiteracy.” In: *GigaScience* 8.5 (May 1, 2019). ISSN: 2047-217X. DOI: 10.1093/gigascience/giz002. URL: <https://doi.org/10.1093/gigascience/giz002> (visited on 06/15/2021).
 - [36] R Leeb et al. “BCI Competition 2008 – Graz data set B.” In: (2008), p. 6.
 - [37] Albina Li et al. “Towards Paradigm-Independent Brain Computer Interfaces.” In: Feb. 1, 2020, pp. 1–6. DOI: 10.1109/BCI48061.2020.9061657.
 - [38] Ke Liao et al. “Decoding Individual Finger Movements from One Hand Using Human EEG Signals.” In: *PLOS ONE* 9.1 (Jan. 8, 2014). Publisher: Public Library of Science, e85192. ISSN: 1932-6203. DOI: 10.1371/journal.pone.0085192. URL: <https://journals.plos.org/plosone/article?id=10.1371/journal.pone.0085192> (visited on 05/18/2021).
 - [39] F. Lotte et al. “A review of classification algorithms for EEG-based brain-computer interfaces: a 10 year update.” In: *Journal of Neural Engineering* 15.3 (June 2018), p. 031005. ISSN: 1741-2552. DOI: 10.1088/1741-2552/aab2f2.

- [40] Fabien Lotte. “A Tutorial on EEG Signal-processing Techniques for Mental-state Recognition in Brain–Computer Interfaces.” In: *Guide to Brain-Computer Music Interfacing*. Ed. by Eduardo Reck Miranda and Julien Castet. London: Springer, 2014, pp. 133–161. ISBN: 978-1-4471-6584-2. DOI: 10.1007/978-1-4471-6584-2_7. URL: https://doi.org/10.1007/978-1-4471-6584-2_7 (visited on 06/09/2021).
- [41] Fabien Lotte. “Signal Processing Approaches to Minimize or Suppress Calibration Time in Oscillatory Activity-Based Brain–Computer Interfaces.” In: *Proceedings of the IEEE* 103 (June 1, 2015), pp. 871–890. DOI: 10.1109/JPROC.2015.2404941.
- [42] Erik K. St Louis et al. *Appendix 6. A Brief History of EEG*. Publication Title: Electroencephalography (EEG): An Introductory Text and Atlas of Normal and Abnormal Findings in Adults, Children, and Infants [Internet]. American Epilepsy Society, 2016. URL: <https://www.ncbi.nlm.nih.gov/books/NBK390348/> (visited on 02/25/2021).
- [43] Cesar Marquez-Chin, Kathryn Atwell, and Milos R Popovic. “Prediction of specific hand movements using electroencephalographic signals.” In: *The Journal of Spinal Cord Medicine* 40.6 (Nov. 2017), pp. 696–705. ISSN: 1079-0268. DOI: 10.1080/10790268.2017.1369215. URL: <https://www.ncbi.nlm.nih.gov/pmc/articles/PMC5778933/> (visited on 05/18/2021).
- [44] Dennis McFarland, A. Lefkowicz, and Jonathan Wolpaw. “Design and operation of an EEG-based brain-computer interface (BCI) with digital signal processing technology.” In: *Behavior Research Methods, Instruments, & Computers* 29 (Sept. 1, 1997), pp. 337–345. DOI: 10.3758/BF03200585.
- [45] Dennis J. McFarland, William A. Sarnacki, and Jonathan R. Wolpaw. “Electroencephalographic (EEG) control of three-dimensional movement.” In: *Journal of Neural Engineering* 7.3 (June 2010), p. 036007. ISSN: 1741-2552. DOI: 10.1088/1741-2560/7/3/036007.

- [46] José del R. Millán et al. *Non-Invasive Brain-Machine Interaction*. International Journal of Pattern Recognition and Artificial Intelligence. ISSN: 0218-0014 Issue: 5 Number: ARTICLE Pages: 959-972 Publisher: World Scientific Publishing Volume: 22. 2008. DOI: 10 . 1142 / S0218001408006600. URL: [http : / / infoscience . epfl . ch / record / 137249](http://infoscience.epfl.ch/record/137249) (visited on 02/25/2021).
- [47] Kai J. Miller, Dora Hermes, and Nathan P. Staff. “The current state of electrocorticography-based brain–computer interfaces.” In: *Neurosurgical Focus* 49.1 (July 1, 2020). Publisher: American Association of Neurological Surgeons Section: Neurosurgical Focus, E2. ISSN: 1092-0684. DOI: 10 . 3171 / 2020 . 4 . FOCUS20185. URL: [https : / / thejns . org / focus / view / journals / neurosurg - focus / 49 / 1 / article - pE2 . xml](https://thejns.org/focus/view/journals/neurosurg-focus/49/1/article-pE2.xml) (visited on 02/25/2021).
- [48] I. Navarro, B. Hubais, and F. Sepulveda. “A Comparison of Time, Frequency and ICA Based Features and Five Classifiers for Wrist Movement Classification in EEG Signals.” In: *2005 IEEE Engineering in Medicine and Biology 27th Annual Conference*. 2005 IEEE Engineering in Medicine and Biology 27th Annual Conference. ISSN: 1558-4615. Jan. 2005, pp. 2118–2121. DOI: 10.1109/IEMBS.2005.1616878.
- [49] Luis Fernando Nicolas-Alonso and Jaime Gomez-Gil. “Brain computer interfaces, a review.” In: *Sensors (Basel, Switzerland)* 12.2 (2012), pp. 1211–1279. ISSN: 1424-8220. DOI: 10 . 3390 / s120201211.
- [50] Natasha Padfield et al. “EEG-Based Brain-Computer Interfaces Using Motor-Imagery: Techniques and Challenges.” In: *Sensors (Basel, Switzerland)* 19.6 (Mar. 22, 2019). ISSN: 1424-8220. DOI: 10 . 3390 / s19061423. URL: [https : / / www . ncbi . nlm . nih . gov / pmc / articles / PMC6471241 /](https://www.ncbi.nlm.nih.gov/pmc/articles/PMC6471241/) (visited on 06/13/2021).
- [51] Konstantinos J. Panoulas, Leontios J. Hadjileontiadis, and Stavros M. Panas. “Brain-Computer Interface (BCI): Types, Processing Perspectives and Applications.” In: *Multimedia Services in Intelligent Environments: Integrated Systems*. Ed. by George

- A. Tsihrintzis and Lakhmi C. Jain. Smart Innovation, Systems and Technologies. Berlin, Heidelberg: Springer, 2010, pp. 299–321. ISBN: 978-3-642-13396-1. DOI: 10.1007/978-3-642-13396-1_14. URL: https://doi.org/10.1007/978-3-642-13396-1_14 (visited on 02/25/2021).
- [52] G. Pfurtscheller and F. H. Lopes da Silva. “Event-related EEG/MEG synchronization and desynchronization: basic principles.” In: *Clinical Neurophysiology: Official Journal of the International Federation of Clinical Neurophysiology* 110.11 (Nov. 1999), pp. 1842–1857. ISSN: 1388-2457. DOI: 10.1016/s1388-2457(99)00141-8.
- [53] G. Pfurtscheller et al. “Mu rhythm (de)synchronization and EEG single-trial classification of different motor imagery tasks.” In: *NeuroImage* 31.1 (May 15, 2006), pp. 153–159. ISSN: 1053-8119. DOI: 10.1016/j.neuroimage.2005.12.003.
- [54] Gert Pfurtscheller and Christa Neuper. “Motor imagery activates primary sensorimotor area in humans.” In: *Neuroscience letters* 239.2 (1997). Place: Shannon Publisher: Elsevier Ireland Ltd, Elsevier, pp. 65–68. ISSN: 0304-3940. DOI: 10.1016/S0304-3940(97)00889-6.
- [55] Gert Pfurtscheller et al. “‘Thought’-control of functional electrical stimulation to restore hand grasp in a patient with tetraplegia.” In: *Neuroscience Letters* 351.1 (Nov. 6, 2003), pp. 33–36. ISSN: 0304-3940. DOI: 10.1016/S0304-3940(03)00947-9.
- [56] Rabie A. Ramadan and Athanasios V. Vasilakos. “Brain computer interface: control signals review.” In: *Neurocomputing* 223 (Feb. 5, 2017), pp. 26–44. ISSN: 0925-2312. DOI: 10.1016/j.neucom.2016.10.024. URL: <https://www.sciencedirect.com/science/article/pii/S0925231216312152> (visited on 02/25/2021).
- [57] H. Ramoser, J. Muller-Gerking, and G. Pfurtscheller. “Optimal spatial filtering of single trial EEG during imagined hand movement.” In: *IEEE Transactions on Rehabilitation Engineering* 8.4 (Dec. 2000). Conference Name: IEEE Transactions on Rehabilita-

- tion Engineering, pp. 441–446. ISSN: 1558-0024. DOI: 10.1109/86.895946.
- [58] Mouad Riyad, Mohammed Khalil, and Abdellah Adib. “MI-EEGNET: A novel convolutional neural network for motor imagery classification.” In: *Journal of Neuroscience Methods* 353 (Apr. 1, 2021), p. 109037. ISSN: 0165-0270. DOI: 10.1016/j.jneumeth.2020.109037. URL: <https://www.sciencedirect.com/science/article/pii/S016502702030460X> (visited on 05/20/2021).
- [59] Germán Rodríguez-Bermúdez and Pedro J. García-Laencina. “Automatic and adaptive classification of electroencephalographic signals for brain computer interfaces.” In: *Journal of Medical Systems* 36 Suppl 1 (Nov. 2012), S51–63. ISSN: 0148-5598. DOI: 10.1007/s10916-012-9893-4.
- [60] Yannick Roy et al. “Deep learning-based electroencephalography analysis: a systematic review.” In: *Journal of neural engineering* 16.5 (2019). Place: England Publisher: IOP Publishing, pp. 051001–051001. ISSN: 1741-2560. DOI: 10.1088/1741-2552/ab260c.
- [61] Simanto Saha et al. “Progress in Brain Computer Interface: Challenges and Opportunities.” In: *Frontiers in Systems Neuroscience* 15 (2021). Publisher: Frontiers. ISSN: 1662-5137. DOI: 10.3389/fnsys.2021.578875. URL: <https://www.frontiersin.org/articles/10.3389/fnsys.2021.578875/full> (visited on 06/13/2021).
- [62] Siavash Sakhavi, Cuntai Guan, and Shuicheng Yan. “Parallel convolutional-linear neural network for motor imagery classification.” In: *2015 23rd European Signal Processing Conference (EUSIPCO)*. 2015 23rd European Signal Processing Conference (EUSIPCO). Nice: IEEE, Aug. 2015, pp. 2736–2740. ISBN: 978-0-9928626-3-3. DOI: 10.1109/EUSIPCO.2015.7362882. URL: <http://ieeexplore.ieee.org/document/7362882/> (visited on 06/14/2021).

- [63] Saeid Sanei. *Adaptive Processing of Brain Signals*. Hoboken: John Wiley & Sons, Incorporated, Wiley-Blackwell, 2013. ISBN: 978-0-470-68613-3.
- [64] Claudia Sannelli et al. “Common Spatial Pattern Patches - an Optimized Filter Ensemble for Adaptive Brain-Computer Interfaces.” In: *Conference proceedings : ... Annual International Conference of the IEEE Engineering in Medicine and Biology Society. IEEE Engineering in Medicine and Biology Society. Conference 2010* (Aug. 1, 2010), pp. 4351–4. DOI: 10.1109/IEMBS.2010.5626227.
- [65] Gerwin Schalk et al. “BCI2000: a general-purpose brain-computer interface (BCI) system.” In: *IEEE transactions on bio-medical engineering* 51.6 (June 2004), pp. 1034–1043. ISSN: 0018-9294. DOI: 10.1109/TBME.2004.827072.
- [66] Robin Tibor Schirrmeister et al. “Deep learning with convolutional neural networks for EEG decoding and visualization.” In: *Human Brain Mapping* 38.11 (2017). _eprint: <https://onlinelibrary.wiley.com/doi/pdf/10.1002/hbm.23730>, pp. 5391–5420. ISSN: 1097-0193. DOI: 10.1002/hbm.23730. URL: <https://onlinelibrary.wiley.com/doi/abs/10.1002/hbm.23730> (visited on 06/15/2021).
- [67] Alois Schlogl et al. “Evaluation Criteria for BCI Research.” In: (2007), p. 66.
- [68] Alois Schlögl et al. “Characterization of four-class motor imagery EEG data for the BCI-competition 2005.” In: *Journal of Neural Engineering* 2.4 (Dec. 2005), pp. L14–22. ISSN: 1741-2560. DOI: 10.1088/1741-2560/2/4/L02.
- [69] Piotr Stawicki et al. “A Novel Hybrid Mental Spelling Application Based on Eye Tracking and SSVEP-Based BCI.” In: *Brain Sciences* 7.4 (Apr. 5, 2017). ISSN: 2076-3425. DOI: 10.3390/brainsci7040035.
- [70] David Steyrl, Reinmar J. Kobler, and Gernot R. Müller-Putz. “On Similarities and Differences of Invasive and Non-Invasive Electrical Brain Signals in Brain-Computer Interfacing.” In:

- Journal of Biomedical Science and Engineering* 9.8 (June 30, 2016). Number: 8 Publisher: Scientific Research Publishing, pp. 393–398. DOI: 10.4236/jbise.2016.98034. URL: <http://www.scirp.org/Journal/Paperabs.aspx?paperid=67876> (visited on 02/25/2021).
- [71] Cathy Stinear et al. “Kinesthetic, but not visual, motor imagery modulates corticomotor excitability.” In: *Experimental brain research. Experimentelle Hirnforschung. Expérimentation cérébrale* 168 (Feb. 1, 2006), pp. 157–64. DOI: 10.1007/s00221-005-0078-y.
- [72] Kaori Suefusa and Toshihisa Tanaka. “A comparison study of visually stimulated brain-computer and eye-tracking interfaces.” In: *Journal of Neural Engineering* 14.3 (June 2017), p. 036009. ISSN: 1741-2552. DOI: 10.1088/1741-2552/aa6086.
- [73] Michael Tangermann et al. “Review of the BCI Competition IV.” In: *Frontiers in Neuroscience* 6 (2012). Publisher: Frontiers. ISSN: 1662-453X. DOI: 10.3389/fnins.2012.00055. URL: <https://www.frontiersin.org/articles/10.3389/fnins.2012.00055/full> (visited on 06/09/2021).
- [74] *The international 10–20 system of EEG electrode placement overlaid on...* ResearchGate. URL: https://www.researchgate.net/figure/The-international-10-20-system-of-EEG-electrode-placement-overlaid-on-the-somatotopic_fig2_281319811 (visited on 04/26/2021).
- [75] Koutroumbas Konstantinos Theodoridis Sergios. *Pattern Recognition*. Elsevier, 2009. ISBN: 978-1-59749-272-0. DOI: 10.1016/B978-1-59749-272-0.X0001-2. URL: <https://linkinghub.elsevier.com/retrieve/pii/B9781597492720X00012> (visited on 06/14/2021).
- [76] J J Vidal. “Toward Direct Brain-Computer Communication.” In: *Annual Review of Biophysics and Bioengineering* 2.1 (1973). _eprint: <https://doi.org/10.1146/annurev.bb.02.060173.001105>, pp. 157–180. DOI: 10.1146/annurev.bb.02.060173.001105. URL:

<https://doi.org/10.1146/annurev.bb.02.060173.001105> (visited on 02/25/2021).

- [77] Stephan Waldert. “Invasive vs. Non-Invasive Neuronal Signals for Brain-Machine Interfaces: Will One Prevail?” In: *Frontiers in Neuroscience* 10 (June 27, 2016). ISSN: 1662-4548. DOI: 10.3389/fnins.2016.00295. URL: <https://www.ncbi.nlm.nih.gov/pmc/articles/PMC4921501/> (visited on 02/25/2021).
- [78] Jonathan R. Wolpaw et al. “Brain–computer interfaces for communication and control.” In: *Clinical Neurophysiology* 113.6 (2002). Place: Shannon Publisher: Elsevier Ireland Ltd, Elsevier Science, pp. 767–791. ISSN: 1388-2457. DOI: 10.1016/S1388-2457(02)00057-3.
- [79] Xinyi Yong and Carlo Menon. “EEG Classification of Different Imaginary Movements within the Same Limb.” In: *PLoS ONE* 10.4 (Apr. 1, 2015). ISSN: 1932-6203. DOI: 10.1371/journal.pone.0121896. URL: <https://www.ncbi.nlm.nih.gov/pmc/articles/PMC4382224/> (visited on 05/18/2021).
- [80] Dariusz Zapała et al. “The effects of handedness on sensorimotor rhythm desynchronization and motor-imagery BCI control.” In: *Scientific Reports* 10 (Feb. 7, 2020). ISSN: 2045-2322. DOI: 10.1038/s41598-020-59222-w. URL: <https://www.ncbi.nlm.nih.gov/pmc/articles/PMC7005877/> (visited on 05/15/2021).
- [81] Jiawei Zhang. “Secrets of the Brain: An Introduction to the Brain Anatomical Structure and Biological Function.” In: *arXiv:1906.03314 [cs, q-bio]* (May 30, 2019). arXiv: 1906.03314. URL: <http://arxiv.org/abs/1906.03314> (visited on 02/25/2021).
- [82] Qiqi Zhang and Ying Liu. “Improving brain computer interface performance by data augmentation with conditional Deep Convolutional Generative Adversarial Networks.” In: *arXiv:1806.07108 [cs, q-bio, stat]* (Dec. 27, 2018). arXiv: 1806.

07108. URL: <http://arxiv.org/abs/1806.07108> (visited on 03/13/2021).